



## Monotonous, symmetric, and nonsymmetric patterns of porous core in vibration study of nano-composite sandwich plate bonded by piezoelectric sheets

M.Pakize <sup>a</sup>, Z.Khoddami Maraghi <sup>b</sup>, M.Irani Rahaghi <sup>a</sup>, S.Niknejad <sup>a</sup>, A.Ghorbanpour Arani <sup>a,c,\*</sup>

<sup>a</sup> Department of Solid Mechanics, Faculty of Mechanical Engineering, University of Kashan, Kashan, Iran.

<sup>b</sup> Faculty of Engineering, Mahallat Institute of Higher Education, Mahallat, Iran.

<sup>c</sup> Institute of Nanoscience & Nanotechnology, University of Kashan, Kashan, Iran.

### Abstract

This paper deals with the free vibrations of a 5-layer sandwich plate consisting of a sutured porous material core. Two randomly oriented straight single-walled carbon nanotube (CNT) reinforced composites and face sheets manufactured of piezoelectric material that is subjected to an external electric voltage, are placed on a Visco-Pasternak foundation. The relationship between strain and stress in the core is expressed by considering the pore fluid pressure based on the Biot theory, and for pore distribution along the core thickness, three uniform, symmetric and nonsymmetric patterns are considered. A quasi-3D sinusoidal shear deformation theory which that couples the effects of shear strain and normal deformation without the need for any shear correction factor which uses Hamilton's principle and Navier's method is used to derive the governing equations of the sandwich structure for the simply supported case. Effects of different parameters on the natural frequencies of the plate are studied including layer thickness ratio, porosity parameter, porosity distribution pattern, pores compressibility, the volume fraction of CNTs and external voltage. The maximum frequency in different modes could be an important design factor that is calculated based on the type of the porosity distribution. Controlling the material properties based on specific needs is the most important advantage of the 5-layer sandwich structure. This paper introduces sandwich panels with porous cores, nanocomposite layers and piezoelectric overlays for the first time which is analyzed to determine system vibration frequencies under external voltage and by changing various parameters with emphasis on different porosity distributions. The frequency of monotonous distribution was 4% higher than symmetric and asymmetric distributions for a constant porosity.

**Keywords:** Free vibration; Sandwich plate; Quasi-3D plate theory; Sutured porous material; Carbon nanotube; Mori-Tanaka approach; Visco-Pasternak foundation

## 1. Introduction

Porous media have desirable characteristics such as being lightweight and highly flexible, sound and energy absorption, and cost-effectiveness. Therefore, they are the favorite materials among aeronautical, mechanical, and civil engineers. In recent years, researchers have considered the effect of the fluid inside the porous medium cavities under the topic of saturated porous media and investigated the structural behaviour of this material. In FG porous structures, the porosity of the structure varies from one surface to the other. Many researchers have studied the behavior of FG structures [1-5]. Most of the current studies about FG porous structures are concentrated on the static, buckling, and vibration analyses which some of them which are mentioned here.

Al Rjoub and Hamad [6] studied the dynamic behaviour of a functionally graded Timoshenko beam analytically. By solving the transport matrix, they concluded that the rotational inertia and the coupling between shear deformation and rotational inertia are small and negligible. Chen et al. [7] performed nonlinear and post-buckling vibration analysis of a graphene nanocomposite functionally graded porous beam. The multilayer beam was formed from a porous metal foam reinforced with graphene platelets (GPLs) so that the pores and the GPL Nanofillers are distributed uniformly in each layer, but the porosity coefficients and the weight fraction of graphene platelets vary from layer to layer according to the thickness direction. Results showed the porosity and GPL distribution effect on increasing the nonlinear frequency and post-buckling load. Zenkour [8] studied the bending responses of single-layer porous and sandwich plates using the quasi-3D shear deformation model by considering the shear strain and normal deformation effects under the effect of the exponent grade and porosity. Subsequently, Arshid et al. [9] studied the free vibration of a circular plate made from a porous media with piezoelectric actuator patches. Due to the thinness of the plate, the shear deformations were neglected. Using the classical plate theory, the Hamilton principle was applied to obtain the equations of motion for the structure, and the effect of some parameters such as the porosity thickness ratio, porosity distribution, and pores compressibility and their influence on the system frequency was analyzed. Safaei et al. [10] studied the thermoelastic behaviour of sandwich panels with polymer porous core and nanocomposite layers reinforced with carbon nanotubes with a polymer matrix. The distribution of pores in the core and the carbon nanotubes on the surface were considered as functionally graded in the thickness direction. The results showed that the sandwich panel with a functionally graded porous core has a smaller deformation than cores with uniform distribution. Arshid et al. [11] studied the static and dynamic analysis of a circular nanocomposite porous microplate reinforced with functionally graded graphene plates using the modified strain gradient theory. To obtain the nanocomposite properties, the Halpin-Tsai method was used and the governing equations were solved with the generalized differential quadrature method with various boundary conditions. They reported that by increasing the porosity factor, the natural frequencies and critical buckling load decrease, while the microplate deformation increases. Gao et al. [12] studied wave propagation in functionally graded porous plates reinforced with graphene plates. In their study, they considered two symmetric non-uniform and one uniform model for the pore distribution and three different patterns for graphene plate distribution in the plate thickness direction. As a result, the mechanical nanocomposite characteristics were extracted with the Halpin-Tsai method. To mention a similar study, Askari et al. [13] studied the effect of piezoelectricity and porosity distribution on the natural frequencies of smart porous plates. They used the Mindlin plate theory to study the Levy boundary conditions. The numerical results showed that the changes in natural frequencies of the sandwich structure are strongly affected by the porosity distribution model. In addition, the natural frequency increase (due to adding piezoelectric layers) is more noticeable for uniform and asymmetric porosity compared with symmetric distribution cases. Balak et al. [14] studied the free vibration of an elliptic sandwich plate with a composite porous plate on piezoelectric overlays. Based on their study, the most important variable on the vibration frequencies of the said plate were the geometric parameters of the elliptic plate and the material characteristics. Safari et al. [15] published a paper about free electrical-magnetic-thermal vibration of a sandwich Timoshenko beam made from a porous material core and composite reinforced with graphene platelets. To describe this issue further, in their paper, the studied parameters were the material length, temperature variations, different porosity, graphene platelets distribution, and the thickness ratio of layers, and the studied output parameter was the natural frequency of the sandwich structure.

Based on the unique characteristics of carbon nanotubes and graphene sheets, they are an ideal choice for many applications. One of the most important applications of carbon nanotubes is based on their mechanical and thermal characteristics which are their use as reinforcement for composite materials [16-18]. The outstanding and exceptional mechanical, electrical, and thermal characteristics of carbon nanotubes and graphene sheets [19-25] have stimulated researchers to exploit them as a new generation of reinforcing agents for polymers. Numerous studies have been made to analytically and experimentally determine the mechanical properties of nanocomposites.

Other nanotube applications include energy storage, the automobile industry, and aeronautics. Shen [26] proposed the objective-oriented usage of carbon nanotubes in polymer composite for the first time in 2009. In this paper, the

nonlinear flexure of composite plates reinforced with carbon nanotubes in thermal environments was studied. In their study, the effectiveness factor ( $\eta$ ) was considered for nanotubes which were obtained by comparing molecular dynamics with the developed rule of mixture. Ke et al. [27] used the Ritz method to study nonlinear vibrations of functionally graded Timoshenko beams reinforced with carbon nanotubes. Shen [28] studied the post-buckling of cylindrical functionally graded composite shells reinforced with carbon nanotubes in thermal environments under axial load. Results showed that the distribution and volumetric percentage of carbon nanotubes have a strong influence on the buckling load and post-buckling behaviour of shells reinforced with carbon nanotubes. Jam et al. [29] studied the free vibrations of functionally graded cylindrical panels reinforced with curved nanotubes with the 3D elasticity theory. In this paper, the nanotube volumetric percentage was varied across the radius and its mechanical characteristic was found with the developed mixing law. The effect of aspect ratio and nanotube curve on the vibration behaviour was studied. This is consistent with results of previous papers. Pourasghar et al. [30] studied the local aggregation of CNTs on the vibration behaviour of functionally graded reinforced nanocomposite cylinders using 3D elasticity theory. They estimated the mechanical properties using the Eshelby-Mori-Tanaka method for a volumetric element of the nanocomposite and used a 4-parameters of power-law distributions model for the functionally graded nanocomposite. Zhang et al. [31] studied the vibration of a bent plate reinforced with carbon nanotubes. In this paper, different configurations of carbon nanotubes were studied. Zhang and Selim [32] studied the free vibration of a thick laminated composite reinforced with carbon nanotubes based on a higher-order shear deformation theory of Reddy for the first time using a meshless method. They used a meshless method based on the generalized moving least squares – Ritz approximation for solving the numerical method. For calculating the effective composite properties which were reinforced with carbon nanotubes with four types of UD, FG-O, FG-X, and FG-V, the Mori-Tanaka method was used. In the end, the effect of carbon nanotube volumetric fraction and the effect of plate aspect ratio, width to thickness of the plate, and the number of plate layers on the nondimensional natural frequency of the plate were solved for various orientations of carbon nanotubes. Thang et al. [33] used a new method to analyze the nonlinear buckling of composite plates reinforced with defective functionally graded carbon nanotubes under axial compression. Their results showed that the defect has a considerable effect on the nonlinear static behaviour of the plate and the FG-O distribution case has the lowest stiffness compared to other distributions. Moradi and Aghadavoudi [34] used the first-order shear deformation theory and meshless method to calculate the deformation and stress distribution of functionally graded nanocomposite sandwich plates reinforced with defective carbon nanotubes on a Winkler-Pasternak foundation. They studied the effect of arrangement, the number of defects, the volume fraction, boundary conditions, and geometric dimensions on the static analysis of the sandwich plate. Daghigh et al. [35] studied the buckling and nonlocal bending of composite nanoplates reinforced with carbon nanotubes and used the Hamilton principle and Eringen nonlocal elasticity theory and the sinusoidal shear deformation theory and Navier analytic method, the constitutive differential governing equations were solved. They considered the effect of temperature, scale parameter, the volume fraction of carbon nanotubes, and length to thickness ratio of the plate on the static bending and buckling behaviour of the plate. The usage of piezoelectric is increasing as sensors and actuators in automotive, aeronautics, computers, home appliances, and medical sciences.

On the other hand, in recent years, the research on structural vibration control has attracted more and more attention and structure control research has become a hot subject of structural analysis [36-38]. Zenkour [39] presented a hygrothermal analysis of a non-homogeneous piezoelectric elastic cylinder. In this study, the effects of initial temperature, pressure, electrical potential, and moisture were studied. Arefi et al. [40] studied the free vibration of a functionally graded sandwich piezoelectric cylindrical shell. In this paper, the first-order shear deformation theory combined with the nonlinear von Karman translational strain equations were used, and the governing equations of the functionally graded sandwich structure with a core were solved with the analytical Navier method. The functionally graded piezoelectric overlays were used as actuators and sensors. Ghasemi and Jaamialahmadi [41] studied the buckling behaviour of multilayer nanoplates made from graphene with two layers of piezoelectric on top and bottom. Their study was based on nonlocal elasticity theories and shear and normal deformations. They solved the resulting equations with the assumptions of simple supports on all 4 edges analytically and the critical buckling loads were obtained. Arefi and Zenkour [42] conducted a study of free vibration and bending of sandwich microbeam made from graphene with two piezo-magnetolectric overlays. In this study, to enforce the microscale effect, the strain gradient theory was used, and the considered microbeam was placed on a Visco-Pasternak foundation. The magnetic and electric potentials were a mixture of polynomial and cosine functions. Ebrahimi and Hosseini [43] studied the flexoelectric effect on the forced nonlinear vibration of a nanocomposite with functionally graded porous core and piezoelectric overlays subject to electrical voltage and outside parameter excitors. For deriving the governing equation of motion of the sandwich plate which was on a visco-Pasternak foundation, the Mindlin and Kirchoff theories and the Hamilton principle were used. Results showed that the electrical voltage does not influence the vibration of piezoelectric and flexoelectric materials. Arani et al. [44] studied energy harvest via a sandwich beam with laminated composite core and piezoelectric overlays under the effect of external fluid movement. In their study, the fiber angle

had a prominent effect on the structural damping, bending stiffness, natural frequency, and finally the harvested energy. They also realized that the maximum voltage occurs when the fibers have an angle of zero and the least amount occurs at the angle of  $50^\circ$ .

To summarize, in the presented paper, an exact solution is presented for free vibration analysis of a 5-layer simply supported sandwich plate consisting of a sutured porous material core, CNT-reinforced interior layers, and piezoelectric face sheets that are subjected to an external electric voltage resting on a Visco-Pasternak foundation. The porosity of the core is uniformly, symmetrically, and asymmetrically repartitioned through the thickness. For its simplicity and accuracy even at a high volume fraction of inclusions, the Mori-Tanaka approach is applied for estimating the effective moduli of the nanocomposite layers. The accuracy of the presented analysis is confirmed and the influences of various parameters on the natural frequencies of the plate are investigated such as aspect ratio, layer thickness ratio, porosity parameter, porosity distribution pattern, pores compressibility, the volume fraction of CNTs, external voltage, Winkler modulus, shear modulus of the surrounding elastic medium and damping modulus parameter of the foundation.

From the main important applications of this type of sandwich structures that utilize new materials that possess characteristics such as flexibility, strength, controllability and smartness, their use in different parts of airplane wing and UAVs can be mentioned.

## 2. Nomenclature

$a, b, h$	Length, width and thickness of plate	$e_1$	Porosity
$h_c$	Thickness of the core	$\nu$	Poisson's ratio
$h_{nc}$	Thickness of the nanocomposite layers	$\rho$	Density
$h_p$	Thickness of the piezoelectric layers	$E_{ij}$	modulus of elasticity
$u, v, w$	Displacement at the middle surface of the plate ( $z=0$ )	$K_w$	Winkler coefficient
$\phi_x$	Rotations from the middle surface along the x-direction	$K_G$	shear coefficient
$\phi_y$	Rotations from the middle surface along the y-direction	$C_d$	damping coefficient
$\phi_z$	Rotations from the middle surface along the z-direction	$C_{ij}$	elastic coefficient
$u_1, u_2, u_3$	Displacement in x, y and z directions	$U$	strain energy
$\hat{\omega}$	Nondimensional natural frequency	$\lambda$	Lamé coefficient
$\delta_{ij}$	Kronecker delta	$\alpha$	Biot coefficient
$P$	pore fluid pressure	$\lambda_u$	Lamé coefficient for the porous material
$\nu_u$	Poisson's ratio for the porous material	$K_{nc}$	bulk moduli of the CNT-reinforced layer
$G_{nc}$	shear moduli of the CNT-reinforced layer	$G_m$	shear moduli of the isotropic matrix
$K_m$	bulk moduli of the isotropic matrix	$k_r, l_r, m_r, n_r$ and $p_r$	Hill's elastic moduli

D	electric displacement	$k_{ij}$	dielectric coefficients
$e_{ij}$	piezoelectric coefficients	$\Psi$	electric potential function
$\varepsilon_{kk}$	volumetric strain	$W$	work done by non-conservative forces
$B$	Skempton coefficient	$V_m$	volume fraction of the polymer matrix
$V_r$	volume fraction of the CNT reinforcement		

### 3. PROBLEM DESCRIPTION AND THE GOVERNING EQUATIONS

As shown in Fig. 1, the sandwich plate with a total thickness of  $h$ , length of  $a$ , and width of  $b$  is made from 5 layers with saturated porous material core with a thickness of  $h_c$  which is reinforced with carbon nanotube composite with a thickness of  $h_{nc}$  and piezoelectric overlays with a thickness of  $h_p$  which function as actuators are placed on a Visco-Pasternak foundation. As the energy method is used to derive equations, and the total potential energy of the structure should be determined. Considering the stress-strain relation of each layer and using quasi-3D sinusoidal theory, strain and kinetic energy of the porous, nanocomposite, and piezoelectric layers are calculated separately.

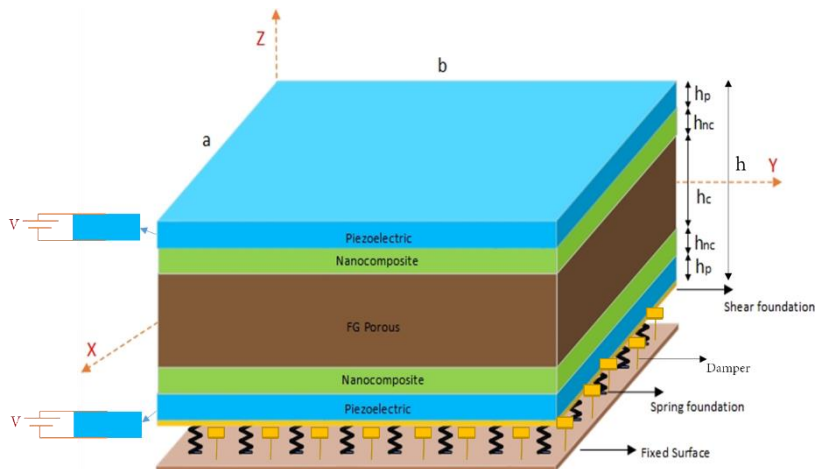


Figure 1. The geometry of the problem.

#### 3.1. Displacement field

The specified displacement field for this structure is a quasi-3D sinusoidal theory proposed by Zenkour [45, 46] in which the stress-free boundary conditions on the top and bottom surfaces of the plate are applied[46]. Using sinusoidal functions was first proposed by Levy[47] and assessed by Stein[48]. The simplicity and accuracy of these functions and the fact that they consider both normal and shear deformations caused Zenkour to use and develop them. Based on the quasi-3D sinusoidal shear deformation theory, components of displacement in a rectangular plate can be considered as [45]

$$\begin{aligned}
u_1(x, y, z, t) &= u(x, y, t) - z \frac{\partial w(x, y, t)}{\partial x} + f(z) \varphi_x(x, y, t) \\
u_2(x, y, z, t) &= v(x, y, t) - z \frac{\partial w(x, y, t)}{\partial y} + f(z) \varphi_y(x, y, t) \\
u_3(x, y, z, t) &= w(x, y, t) + \frac{df(z)}{dz} \varphi_z(x, y, t)
\end{aligned} \tag{1}$$

Where  $u_1$ ,  $u_2$ , and  $u_3$  are displacement in  $x$ ,  $y$  and  $z$  directions respectively, and  $u$ ,  $v$ , and  $w$  show corresponding components of displacement at the middle surface of the plate ( $z=0$ ).  $\varphi_x$  and  $\varphi_y$  represent rotations around  $y$  and  $x$ -axes, respectively,  $\varphi_z$  is an unknown function and  $f(z)$  is defined as the following [49, 50]:

$$f(z) = \frac{h}{\pi} \sin\left(\frac{\pi z}{h}\right) \tag{2}$$

Based on the strain-displacement relations in  $x$ - $y$ - $z$  coordinates, the components of the strain can be calculated using Eq. (1) as [51]

$$\begin{aligned}
\varepsilon_{xx} &= \frac{\partial u_1}{\partial x} = \frac{\partial u}{\partial x} - z \frac{\partial^2 w}{\partial x^2} + f(z) \frac{\partial \varphi_x}{\partial x} \\
\varepsilon_{yy} &= \frac{\partial u_2}{\partial y} = \frac{\partial v}{\partial y} - z \frac{\partial^2 w}{\partial y^2} + f(z) \frac{\partial \varphi_y}{\partial y} \\
\varepsilon_{zz} &= \frac{\partial u_3}{\partial z} = \frac{d^2 f}{dz^2} \varphi_z \\
\gamma_{yz} &= \frac{\partial u_2}{\partial z} + \frac{\partial u_3}{\partial y} = \frac{df(z)}{dz} \left( \varphi_y + \frac{\partial \varphi_z}{\partial y} \right) \\
\gamma_{xz} &= \frac{\partial u_1}{\partial z} + \frac{\partial u_3}{\partial x} = \frac{df(z)}{dz} \left( \varphi_x + \frac{\partial \varphi_z}{\partial x} \right) \\
\gamma_{xy} &= \frac{\partial u_1}{\partial y} + \frac{\partial u_2}{\partial x} = \frac{\partial u}{\partial y} + \frac{\partial v}{\partial x} + f(z) \left( \frac{\partial \varphi_x}{\partial y} + \frac{\partial \varphi_y}{\partial x} \right) - 2z \frac{\partial^2 w}{\partial x \partial y}
\end{aligned} \tag{3}$$

### 3.2 Porous core

Porous materials are a class of nonhomogeneous materials that have attained a considerable reduction in weight due to the presence of pores. Due to the low strength of these materials, they aren't typically used alone but used as a core in a sandwich structure. For a nonhomogeneous porous core, the mechanical properties of the material include modulus of elasticity ( $E$ ), shear modulus ( $G$ ), and density ( $\rho$ ), which may have monotonous, symmetric, and nonsymmetric distributions as shown in the figure below [9].

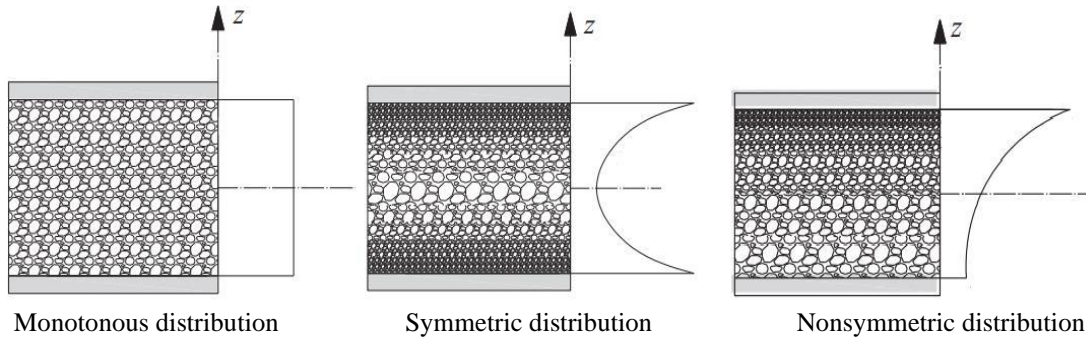


**Figure 2. Distribution patterns of pores [52]**

For the monotonous distribution:

$$\begin{aligned}
 E_c(z) &= E_1 [1 - e_1] \\
 G_c(z) &= G_1 [1 - e_1] \\
 \rho_c(z) &= \rho_1 [1 - e_1]
 \end{aligned} \tag{4}$$

Symmetric distribution means that the following equations apply:

$$\begin{aligned}
 E_c(z) &= E_1 \left[ 1 - e_1 \cos\left(\frac{\pi z}{h_c}\right) \right] \\
 G_c(z) &= G_1 \left[ 1 - e_1 \cos\left(\frac{\pi z}{h_c}\right) \right] \\
 \rho_c(z) &= \rho_1 \left[ 1 - e_1 \cos\left(\frac{\pi z}{h_c}\right) \right]
 \end{aligned} \tag{5}$$

Nonsymmetric distribution:

$$\begin{aligned}
 E_c(z) &= E_1 \left[ 1 - e_1 \cos\left(\frac{\pi z}{2h_c} + \frac{\pi}{4}\right) \right] \\
 G_c(z) &= G_1 \left[ 1 - e_1 \cos\left(\frac{\pi z}{2h_c} + \frac{\pi}{4}\right) \right] \\
 \rho_c(z) &= \rho_1 \left[ 1 - e_1 \cos\left(\frac{\pi z}{2h_c} + \frac{\pi}{4}\right) \right]
 \end{aligned} \tag{6}$$

In these relationships,  $E_1$ ,  $G_1$  and  $\rho_1$  indicated the considered property in the case without any pores, and the dimensionless coefficient ( $e_1$ ) is the porosity. It should be mentioned that in porous materials, the Poisson's ratio ( $\nu$ ) is considered as a constant. Due to the isotropy of these materials, the following relationship between elastic modulus, shear modulus, and Poisson ratio applies [9].

Based on Hook's law, the relationship between stress components and strain components in the solid material in the elastic range is given by the following equation [51]

$$\sigma_{ij}(z) = 2G \varepsilon_{ij} + \lambda \varepsilon_{kk} \delta_{ij} \quad (7)$$

Wherein  $\lambda$  is the Lamé coefficient,  $\delta_{ij}$  is the Kronecker delta, and  $\varepsilon_{kk}$  is the volumetric strain. These variables are defined via the following formulas [51].

$$\lambda = \frac{E\nu}{(1+\nu)(1-2\nu)} = \frac{2\nu}{1-2\nu}G, \quad \delta_{ij} = \begin{cases} 1 & i = j \\ 0 & i \neq j \end{cases}, \quad \varepsilon_{kk} = \varepsilon_{xx} + \varepsilon_{yy} + \varepsilon_{zz} \quad (8)$$

Research about the relationship between strain and stress in porous materials was done by Biot which included 2 main assumptions in his theory [53]:

- Increasing pore pressure results in the expansion of the material.
- Applying compressive load on the pores elevates the pore pressure.

Based on these assumptions, in porous materials filled with fluid (saturated porous materials), the stress and strain are interconnected based on the following relationship:

$$\sigma_{ij} = 2G \varepsilon_{ij} + \lambda_u \varepsilon_{kk} \delta_{ij} - \alpha p \delta_{ij} \quad i, j = 1, 2, 3 \quad (9)$$

In this relationship,  $p$  is the pore fluid pressure.  $\alpha$  is known as the Biot coefficient of effective stress and  $\lambda$  is the Lamé coefficient for the porous material. This coefficient is computed from the following relationships [9].

$$\lambda_u = \frac{2\nu_u}{1-2\nu_u}G, p = M (\xi - \alpha \varepsilon_{kk}) \quad (10)$$

In this relationship,  $\xi$  is the fluid volume in the pores. This coefficient is a function of the available space inside the pore and when the pores are filled with fluid (for the undrained material case), the value is equal to zero.

Also,  $\nu \leq \nu_u < 0.5$  is the Poisson's ratio for the porous material, and  $M$  is known as the Biot modulus which is computed by the following equations.

$$\nu_u = \frac{3\nu + \alpha B (1-2\nu)}{3 - \alpha B (1-2\nu)}G, M = \frac{2(\nu_u - \nu)}{\alpha^2 (1-2\nu_u)(1-2\nu)}G \quad (11)$$

In this relationship, the nondimensional variable  $0 \leq B < 1$  is the Skempton coefficient. This coefficient shows the compressibility of the fluid inside the pores so that  $B=0$  represents incompressible fluid and  $B=1$  represents fully compressible fluid. Therefore, the relationships  $\nu_u = \nu, \lambda_u = \lambda, M = 0, p = 0$  from the Biot law stated in Eq.

(9) for solid materials containing fluid are changed to the Hook's law stated in Eq. (7).

As it was mentioned, for porous saturated materials,  $\xi = 0$  holds, therefore the pore pressure can be calculated by Eq. (10).

$$p = -M \alpha \varepsilon_{kk} \tag{12}$$

By substituting Eq. (12) in Eq. (9) the following relationship can be obtained.

$$\sigma_{ij} (z) = 2G \varepsilon_{ij} + (\lambda_u + M \alpha^2) \varepsilon_{kk} \delta_{ij} \tag{13}$$

For the porous core following relation between stress and strain tensors can be considered.

$$\begin{pmatrix} \sigma_{xx} \\ \sigma_{yy} \\ \sigma_{zz} \\ \tau_{yz} \\ \tau_{xz} \\ \tau_{xy} \end{pmatrix} = \begin{bmatrix} C_{11}^c & C_{12}^c & C_{13}^c & 0 & 0 & 0 \\ C_{21}^c & C_{22}^c & C_{23}^c & 0 & 0 & 0 \\ C_{31}^c & C_{32}^c & C_{33}^c & 0 & 0 & 0 \\ 0 & 0 & 0 & C_{44}^c & 0 & 0 \\ 0 & 0 & 0 & 0 & C_{55}^c & 0 \\ 0 & 0 & 0 & 0 & 0 & C_{66}^c \end{bmatrix} \begin{pmatrix} \varepsilon_{xx} \\ \varepsilon_{yy} \\ \varepsilon_{zz} \\ \gamma_{yz} \\ \gamma_{xz} \\ \gamma_{xy} \end{pmatrix} \tag{14}$$

In which  $\gamma_{ij}=2\varepsilon_{ij}$  indicates the shear strain and

$$\begin{aligned} C_{11}^c &= C_{22}^c = C_{33}^c = \frac{(1-\nu_{uc})E_c(z)}{(1+\nu_c)(1-2\nu_{uc})} + \left( \frac{(\nu_{uc}-\nu_c)}{(1-2\nu_c)(1-2\nu_{uc})} \right) \cdot \frac{E_c(z)}{(1+\nu_c)} \\ C_{12}^c &= C_{21}^c = C_{13}^c = C_{31}^c = C_{23}^c = C_{32}^c = \frac{\nu_{uc}E_c(z)}{(1+\nu_c)(1-2\nu_{uc})} \\ C_{44}^c &= C_{55}^c = C_{66}^c = G_c(z) = \frac{E_c(z)}{2(1+\nu_c)} \end{aligned} \tag{15}$$

Where  $E_c(z)$ ,  $G_c(z)$  and  $\nu_c$  are elasticity modulus, shear modulus and Poisson’s ratio of the porous cores, respectively.

It should be noted that the proelastic relationships mentioned for the porous materials are completely based on the assumptions of the limitations stated below

- Linearity of the stress-strain relationship
- Irreversibility of the deformation process meaning that no energy is lost in a complete closed loop

### 3.3 CNT-reinforced layers

As shown in Fig. 1. The porous core is surrounded by two CNT-reinforced layers. The CNTs are distributed uniformly with randomly orientated directions. According to the rule of mixture, the density of a CNT-reinforced polymer can be calculated as follow:

$$\rho = \rho_m V_m + \rho_r V_r, \quad (16)$$

In which  $\rho$  and  $V$  indicate density and volume fraction, while subscripts  $m$  and  $r$  indicate polymer matrix and CNT reinforcement, respectively.

Also, the volume fraction of the polymer matrix can be obtained using the following relation:

$$V_m = 1 - V_r. \quad (17)$$

As the CNTs are orientated randomly, the CNT-reinforced matrix can be considered as an isotropic structure and Eq. (14) can be used for CNT-reinforced layers as well, wherein the following relationships hold:

$$\begin{aligned} C_{11}^{nc} = C_{22}^{nc} = C_{33}^{nc} &= \frac{(1 - \nu_{nc}) E_{nc}}{(1 + \nu_{nc})(1 - 2\nu_{nc})} \\ C_{12}^{nc} = C_{21}^{nc} = C_{13}^{nc} = C_{31}^{nc} = C_{23}^{nc} = C_{32}^{nc} &= \frac{\nu_{nc} E_{nc}}{(1 + \nu_{nc})(1 - 2\nu_{nc})} \\ C_{44}^{nc} = C_{55}^{nc} = C_{66}^{nc} = G_{nc} &= \frac{E_{nc}}{2(1 + \nu_{nc})} \end{aligned} \quad (18)$$

Where elastic modulus ( $E_{nc}$ ) and Poisson's ratio ( $\nu_{nc}$ ) of the CNT-reinforced layers can be estimated using the Eshelby–Mori–Tanaka scheme via

$$E_{nc} = \frac{9K_{nc}G_{nc}}{3K_{nc} + G_{nc}}, \quad \nu_{nc} = \frac{3K_{nc} - 2G_{nc}}{6K_{nc} + 2G_{nc}}, \quad (19)$$

In which  $G_{nc}$  and  $K_{nc}$  are shear and bulk moduli of the CNT-reinforced layers respectively and can be calculated based on the Eshelby–Mori–Tanaka scheme as described below [54, 55]:

$$K_{nc} = K_m + \frac{(\delta_r - 3K_m\alpha_r)V_r}{3(V_m + V_r\alpha_r)} \quad G_{nc} = G_m + \frac{(\eta_r - 2G_m\beta_r)V_r}{2(V_m + V_r\beta_r)} \quad (20)$$

In which  $G_m$  and  $K_m$  stand for shear and bulk moduli of the isotropic matrix which can be evaluated via:

$$G_m = \frac{E_m}{2(1 + \nu_m)}, \quad K_m = \frac{E_m}{3(1 - 2\nu_m)}, \quad (21)$$

Where  $E_m$  and  $\nu_m$  are elasticity modulus and Poisson's ratio of the isotropic matrix and  $\alpha_r$ ,  $\beta_r$ ,  $\delta_r$  and  $\eta_r$  are defined as the following relationship [56]:

$$\begin{aligned}
 \alpha_r &= \frac{3(K_m + G_m) + k_r + l_r}{3(G_m + k_r)}, \\
 \beta_r &= \frac{1}{5} \left[ \frac{4G_m + 2k_r + l_r}{3(G_m + k_r)} + \frac{4G_m}{G_m + p_r} + \frac{4G_m(3K_m + 4G_m)}{G_m(3K_m + G_m) + m_r(3K_m + 7G_m)} \right], \\
 \delta_r &= \frac{1}{3} \left[ n_r + 2l_r + \frac{(2k_r + l_r)(3K_m + G_m - l_r)}{G_m + k_r} \right], \\
 \eta_r &= \frac{1}{5} \left[ \frac{2}{3}(n_r - l_r) + \frac{8G_m p_r}{G_m + p_r} + \frac{2(k_r - l_r)(2G_m + l_r)}{3(G_m + k_r)} + \frac{8m_r G_m(3K_m + 4G_m)}{3K_m(G_m + m_r) + G_m(G_m + 7m_r)} \right],
 \end{aligned} \tag{22}$$

In Eq. (22),  $k_r$ ,  $l_r$ ,  $m_r$ ,  $n_r$  and  $p_r$  are five independent constants known as Hill’s elastic moduli [56].

### 3.4. Piezoelectric layers

For the piezoelectric face sheets, stress-strain relation can be written as the following formula [57]:

$$\begin{Bmatrix} \sigma_{xx} \\ \sigma_{yy} \\ \sigma_{zz} \\ \tau_{yz} \\ \tau_{xz} \\ \tau_{xy} \end{Bmatrix} = \begin{bmatrix} C_{11}^p & C_{12}^p & C_{13}^p & 0 & 0 & 0 \\ C_{12}^p & C_{22}^p & C_{13}^p & 0 & 0 & 0 \\ C_{13}^p & C_{13}^p & C_{33}^p & 0 & 0 & 0 \\ 0 & 0 & 0 & C_{44}^p & 0 & 0 \\ 0 & 0 & 0 & 0 & C_{55}^p & 0 \\ 0 & 0 & 0 & 0 & 0 & C_{66}^p \end{bmatrix} \begin{Bmatrix} \varepsilon_{xx} \\ \varepsilon_{yy} \\ \varepsilon_{zz} \\ \gamma_{yz} \\ \gamma_{xz} \\ \gamma_{xy} \end{Bmatrix} - \begin{bmatrix} 0 & 0 & e_{31} \\ 0 & 0 & e_{32} \\ 0 & 0 & e_{33} \\ 0 & e_{24} & 0 \\ e_{15} & 0 & 0 \\ 0 & 0 & 0 \end{bmatrix} \begin{Bmatrix} E_x \\ E_y \\ E_z \end{Bmatrix} \tag{23-a}$$

$$\begin{Bmatrix} D_x \\ D_y \\ D_z \end{Bmatrix} = \begin{bmatrix} 0 & 0 & 0 & 0 & e_{15} & 0 \\ 0 & 0 & 0 & e_{24} & 0 & 0 \\ e_{31} & e_{32} & e_{33} & 0 & 0 & 0 \end{bmatrix} \begin{Bmatrix} \varepsilon_{xx} \\ \varepsilon_{yy} \\ \varepsilon_{zz} \\ \gamma_{yz} \\ \gamma_{xz} \\ \gamma_{xy} \end{Bmatrix} + \begin{bmatrix} k_{11} & 0 & 0 \\ 0 & k_{22} & 0 \\ 0 & 0 & k_{33} \end{bmatrix} \begin{Bmatrix} E_x \\ E_y \\ E_z \end{Bmatrix} \tag{23-b}$$

Where  $C_{ij}$  are elastic coefficients of the piezoelectric layers,  $e_{ij}$  and  $k_{ij}$  are piezoelectric and dielectric coefficients,  $D$  is electric displacement and  $E_i$  denote electric field which can be calculated using an electric potential function ( $\Psi = \Psi(x, y, z, t)$ ) as

$$E_x = -\frac{\partial \Psi}{\partial x} \quad E_y = -\frac{\partial \Psi}{\partial y} \quad E_z = -\frac{\partial \Psi}{\partial z} \tag{24}$$

In this paper, the following distribution is considered for electric potential function [58]

$$\Psi(x, y, z, t) = \frac{2\Psi_0}{h_p} \tilde{z} - \cos\left(\frac{\pi \tilde{z}}{h_p}\right) \psi(x, y, t) \tag{25}$$

Here,  $\psi_0$  is the electric potential implied on the top and bottom of the plate and

$\psi = \psi(x,y,t)$  is an unspecified function and

$$\tilde{z} = \begin{cases} z_b = z + \frac{h_c}{2} + h_{nc} + \frac{h_p}{2} & \text{Bottom layer} \\ z_t = z - \frac{h_c}{2} - h_{nc} - \frac{h_p}{2} & \text{Top layer} \end{cases} \quad (26)$$

### 3.5. Hamilton's principle

The set of the governing equations can be derived using Hamilton's principle via [59]

$$\int_{t_1}^{t_2} (-\delta U + \delta T + \delta W) dt = 0, \quad (27)$$

In which  $\delta$  is a variational operator,  $[t_1, t_2]$  is the desired time interval,  $U$  is strain energy,  $T$  is kinetic energy and  $W$  is work done due to non-conservative forces.

The strain energy can be calculated as

$$U = \frac{1}{2} \iint_S \left\{ \int_{-\frac{h}{2}}^{-\frac{h_c}{2} - h_{nc}} \left[ \sigma_{xx} \varepsilon_{xx} + \sigma_{yy} \varepsilon_{yy} + \sigma_{zz} \varepsilon_{zz} + \sigma_{xy} \gamma_{xy} + \sigma_{xz} \gamma_{xz} + \sigma_{yz} \gamma_{yz} - (D_x E_x + D_y E_y + D_z E_z) \right] dz + \int_{-\frac{h_c}{2} - h_{nc}}^{-\frac{h_c}{2}} \left( \sigma_{xx} \varepsilon_{xx} + \sigma_{yy} \varepsilon_{yy} + \sigma_{zz} \varepsilon_{zz} + \sigma_{xy} \gamma_{xy} + \sigma_{xz} \gamma_{xz} + \sigma_{yz} \gamma_{yz} \right) dz + \int_{-\frac{h_c}{2}}^{-\frac{h_c}{2} + h_{nc}} \left( \sigma_{xx} \varepsilon_{xx} + \sigma_{yy} \varepsilon_{yy} + \sigma_{zz} \varepsilon_{zz} + \sigma_{xy} \gamma_{xy} + \sigma_{xz} \gamma_{xz} + \sigma_{yz} \gamma_{yz} \right) dz + \int_{-\frac{h_c}{2} + h_{nc}}^{\frac{h}{2}} \left[ \sigma_{xx} \varepsilon_{xx} + \sigma_{yy} \varepsilon_{yy} + \sigma_{zz} \varepsilon_{zz} + \sigma_{xy} \gamma_{xy} + \sigma_{xz} \gamma_{xz} + \sigma_{yz} \gamma_{yz} - (D_x E_x + D_y E_y + D_z E_z) \right] dz \right\} dS \quad (28)$$

In which  $S$  is the plate surface. The kinetic energy can be stated as

$$\begin{aligned}
T = \frac{1}{2} \iint_S \left\{ \int_{-\frac{h}{2}}^{\frac{h_c-h_{nc}}{2}} \rho_p \left[ \left( \frac{\partial u_1}{\partial t} \right)^2 + \left( \frac{\partial u_2}{\partial t} \right)^2 + \left( \frac{\partial u_3}{\partial t} \right)^2 \right] dz + \int_{-\frac{h_c-h_{nc}}{2}}^{\frac{h_c}{2}} \rho_{nc} \left[ \left( \frac{\partial u_1}{\partial t} \right)^2 + \left( \frac{\partial u_2}{\partial t} \right)^2 + \left( \frac{\partial u_3}{\partial t} \right)^2 \right] dz + \right. \\
\left. \int_{-\frac{h_c}{2}}^{\frac{h_c}{2}} \rho_c \left[ \left( \frac{\partial u_1}{\partial t} \right)^2 + \left( \frac{\partial u_2}{\partial t} \right)^2 + \left( \frac{\partial u_3}{\partial t} \right)^2 \right] dz + \int_{\frac{h_c}{2}}^{\frac{h_c+h_{nc}}{2}} \rho_{nc} \left[ \left( \frac{\partial u_1}{\partial t} \right)^2 + \left( \frac{\partial u_2}{\partial t} \right)^2 + \left( \frac{\partial u_3}{\partial t} \right)^2 \right] dz + \right. \\
\left. \int_{\frac{h_c+h_{nc}}{2}}^{\frac{h}{2}} \rho_p \left[ \left( \frac{\partial u_1}{\partial t} \right)^2 + \left( \frac{\partial u_2}{\partial t} \right)^2 + \left( \frac{\partial u_3}{\partial t} \right)^2 \right] dz \right\} dS
\end{aligned} \tag{29}$$

The work done by external electric potential can be written in the form [60]

$$W_{ext} = \frac{1}{2} \iint_S \left( N_{ex} \left( \frac{\partial w}{\partial x} \right)^2 + N_{ey} \left( \frac{\partial w}{\partial y} \right)^2 \right) dS \tag{30}$$

Here, the normal force is induced by electric voltage, which can be written as [60, 61]

$$N_{ex} = \int -e_{31} \frac{2V_0}{h_p} dz, N_{ey} = \int -e_{32} \frac{2V_0}{h_p} dz \tag{31}$$

The work due to external works includes the visco-Pasternak foundation [42, 43]

$$\Sigma_{foundation} = \frac{1}{2} \iint_S \left[ -K_w w + K_G \left( \frac{\partial^2 w}{\partial x^2} + \frac{\partial^2 w}{\partial y^2} \right) - C_d \left( \frac{\partial w}{\partial t} \right) \right] \cdot w dS \tag{32}$$

For this foundation type, the force is defined as:

$$F(x, y) = -K_w w + K_G \left( \frac{\partial^2 w}{\partial x^2} + \frac{\partial^2 w}{\partial y^2} \right) - C_d \left( \frac{\partial w}{\partial t} \right) \tag{33}$$

where  $K_w$ ,  $K_G$  and  $C_d$  are Winkler, shear and damping factors of the Visco-Pasternak foundation, respectively.

Substituting Eqs. (28)-(32) into Eq. (27) leads to the following governing equations:

$$\begin{aligned}
 \delta u &: \frac{\partial N_{xx}}{\partial x} + \frac{\partial N_{xy}}{\partial y} - I_{11} \frac{\partial^2 u}{\partial t^2} - I_{13} \frac{\partial^2 \phi_x}{\partial t^2} + I_{12} \frac{\partial^3 w}{\partial x \partial t^2} = 0 \\
 \delta v &: \frac{\partial N_{yy}}{\partial y} + \frac{\partial N_{xy}}{\partial x} - I_{11} \frac{\partial^2 v}{\partial t^2} - I_{13} \frac{\partial^2 \phi_y}{\partial t^2} + I_{12} \frac{\partial^3 w}{\partial y \partial t^2} = 0 \\
 \delta w &: \frac{\partial^2 M_{xx}}{\partial x^2} + 2 \frac{\partial^2 M_{xy}}{\partial y \partial x} + \frac{\partial^2 M_{yy}}{\partial y^2} - I_{11} \frac{\partial^2 w}{\partial t^2} - J_{13} \frac{\partial^2 \phi_z}{\partial t^2} \\
 &- I_{12} \left( \frac{\partial^3 u}{\partial x \partial t^2} + \frac{\partial^3 v}{\partial y \partial t^2} \right) + I_{22} \left( \frac{\partial^4 w}{\partial x^2 \partial t^2} + \frac{\partial^4 w}{\partial y^2 \partial t^2} \right) - I_{23} \left( \frac{\partial^3 \phi_x}{\partial x \partial t^2} + \frac{\partial^3 \phi_y}{\partial y \partial t^2} \right) \\
 &- K_w w + K_G \left( \frac{\partial^2 w}{\partial x^2} + \frac{\partial^2 w}{\partial y^2} \right) - C_d \left( \frac{\partial w}{\partial t} \right) + N_{ex} \frac{\partial^2 w}{\partial x^2} + N_{ey} \frac{\partial^2 w}{\partial y^2} = 0 \tag{34} \\
 \delta \phi_x &: \frac{\partial Q_{xx}}{\partial x} + \frac{\partial P_{xy}}{\partial y} - P_{xz} - I_{13} \frac{\partial^2 u}{\partial t^2} - I_{33} \frac{\partial^2 \phi_x}{\partial t^2} + I_{23} \frac{\partial^3 w}{\partial x \partial t^2} = 0 \\
 \delta \phi_y &: \frac{\partial Q_{yy}}{\partial y} + \frac{\partial P_{xy}}{\partial x} - P_{yz} - I_{13} \frac{\partial^2 v}{\partial t^2} - I_{33} \frac{\partial^2 \phi_y}{\partial t^2} + I_{23} \frac{\partial^3 w}{\partial y \partial t^2} = 0 \\
 \delta \phi_z &: \frac{\partial P_{yz}}{\partial y} + \frac{\partial P_{xz}}{\partial x} - Q_{zz} - J_{21} \frac{\partial^2 w}{\partial t^2} - J_{22} \frac{\partial^2 \phi_z}{\partial t^2} = 0 \\
 \delta \psi &: \frac{\partial \bar{D}_x}{\partial x} + \frac{\partial \bar{D}_y}{\partial y} + \bar{D}_z = 0
 \end{aligned}$$

In which  $I_{ij}$  and  $J_{ij}$  are defined in Appendix A and

$$\begin{aligned}
 \left\{ \begin{matrix} N_{ij} \\ M_{ij} \\ P_{ij} \end{matrix} \right\} &= \int_{-\frac{h}{2}}^{\frac{h}{2}} \sigma_{ij} \begin{Bmatrix} 1 \\ z \\ \frac{df}{dz} \end{Bmatrix} dz \quad i, j = x, y, z \\
 Q_{ij} &= \int_{-\frac{h}{2}}^{\frac{h}{2}} \sigma_{ij} f(z) dz \quad \bar{D}_i = \int_{-\frac{h}{2}}^{\frac{h}{2}} D_i \cos\left(\frac{\pi z}{h_p}\right) dz \quad i, j = x, y \\
 Q_{zz} &= \int_{-\frac{h}{2}}^{\frac{h}{2}} \sigma_{ij} \frac{d^2 f}{dz^2} dz \quad \bar{D}_z = \frac{h_p}{\pi} \int_{-\frac{h}{2}}^{\frac{h}{2}} D_i \sin\left(\frac{\pi z}{h_p}\right) dz
 \end{aligned} \tag{35}$$

By substituting equations (3), (14), (23), (24) and (25) into equations (34) and (35), the set of the governing equations can be written as

$$\begin{aligned}
\delta u : & \zeta_{31} \frac{\partial \psi}{\partial x} - B_{11} \frac{\partial^3 w}{\partial x^3} + F_{11} \frac{\partial^2 \phi_x}{\partial x^2} + F_{12} \frac{\partial^2 \phi_y}{\partial x \partial y} - B_{12} \frac{\partial^3 w}{\partial y^2 \partial x} \\
& + A_{13} \frac{\partial \phi_z}{\partial x} + A_{11} \frac{\partial^2 u}{\partial x^2} + A_{12} \frac{\partial^2 v}{\partial x \partial y} + F_{66} \frac{\partial^2 \phi_x}{\partial y^2} + F_{66} \frac{\partial^2 \phi_y}{\partial x \partial y} - B_{66} \frac{\partial^3 w}{\partial y^2 \partial x} \\
& + A_{66} \frac{\partial^2 u}{\partial y^2} + A_{66} \frac{\partial^2 v}{\partial x \partial y} - I_{13} \frac{\partial^2 \phi_x}{\partial t^2} + I_{12} \frac{\partial^3 w}{\partial t^2 \partial x} - I_{11} \frac{\partial^2 u}{\partial t^2} = 0 \\
\delta v : & \zeta_{32} \frac{\partial \psi}{\partial y} - B_{22} \frac{\partial^3 w}{\partial y^3} + F_{22} \frac{\partial^2 \phi_y}{\partial y^2} + F_{12} \frac{\partial^2 \phi_x}{\partial x \partial y} - B_{12} \frac{\partial^3 w}{\partial x^2 \partial y} \\
& + A_{23} \frac{\partial \phi_z}{\partial y} + A_{22} \frac{\partial^2 u}{\partial y^2} + A_{12} \frac{\partial^2 u}{\partial x \partial y} + F_{66} \frac{\partial^2 \phi_y}{\partial x^2} + F_{66} \frac{\partial^2 \phi_x}{\partial x \partial y} - B_{66} \frac{\partial^3 w}{\partial x^2 \partial y} \\
& + A_{66} \frac{\partial^2 u}{\partial x^2} + A_{66} \frac{\partial^2 u}{\partial x \partial y} - I_{13} \frac{\partial^2 \phi_y}{\partial t^2} + I_{12} \frac{\partial^3 w}{\partial t^2 \partial y} - I_{11} \frac{\partial^2 v}{\partial t^2} = 0 \\
\delta w : & 2H_{66} \frac{\partial^3 \phi_y}{\partial y \partial x^2} - 2D_{66} \frac{\partial^4 w}{\partial y^2 \partial x^2} + I_{22} \frac{\partial^4 w}{\partial x^2 \partial t^2} - I_{12} \frac{\partial^3 v}{\partial t^2 \partial y} \\
& + I_{22} \frac{\partial^4 w}{\partial y^2 \partial t^2} - D_{11} \frac{\partial^4 w}{\partial x^4} + B_{13} \frac{\partial^2 \phi_z}{\partial x^2} + I_{31} \frac{\partial^2 \psi}{\partial x^2} + 2H_{66} \frac{\partial^3 \phi_x}{\partial x \partial y^2} + B_{66} \frac{\partial^3 u}{\partial y^2 \partial x} \\
& + B_{66} \frac{\partial^3 v}{\partial y \partial x^2} + H_{11} \frac{\partial^3 \phi_x}{\partial x^3} + H_{12} \frac{\partial^3 \phi_y}{\partial y \partial x^2} - 2D_{12} \frac{\partial^4 w}{\partial x^2 \partial y^2} + B_{11} \frac{\partial^3 u}{\partial x^3} + B_{12} \frac{\partial^3 v}{\partial y \partial x^2} \\
& + \mu_{32} \frac{\partial^2 \psi}{\partial y^2} + B_{23} \frac{\partial^2 \phi_z}{\partial y^2} + B_{12} \frac{\partial^3 u}{\partial x \partial y^2} + B_{22} \frac{\partial^3 v}{\partial y^3} + H_{12} \frac{\partial^3 \phi_x}{\partial x \partial y^2} - D_{22} \frac{\partial^4 w}{\partial y^4} \\
& + H_{22} \frac{\partial^3 \phi_y}{\partial y^3} - I_{23} \frac{\partial^3 \phi_x}{\partial t^2 \partial x} - K_w w + K_G \frac{\partial^2 w}{\partial x^2} + K_G \frac{\partial^2 w}{\partial y^2} - C_d \left( \frac{\partial w}{\partial t} \right) \\
& - \Gamma_{31} \frac{2V_0}{h_p} \frac{\partial^2 w}{\partial x^2} - \Gamma_{32} \frac{2V_0}{h_p} \frac{\partial^2 w}{\partial y^2} - I_{11} \frac{\partial^2 w}{\partial t^2} - I_{23} \frac{\partial^3 \phi_y}{\partial t^2 \partial y} - J_{21} \frac{\partial^2 \phi_z}{\partial t^2} - I_{12} \frac{\partial^3 u}{\partial t^2 \partial x} = 0 \\
\delta \phi_x : & \mu_{31} \frac{\partial \psi}{\partial x} - H_{11} \frac{\partial^3 w}{\partial x^3} + F_{66} \frac{\partial^2 v}{\partial y \partial x} + L_{11} \frac{\partial^2 \phi_x}{\partial x^2} - H_{12} \frac{\partial^3 w}{\partial y^2 \partial x} \\
& + F_{13} \frac{\partial \phi_z}{\partial x} + F_{66} \frac{\partial^2 u}{\partial y^2} + F_{12} \frac{\partial^2 v}{\partial x \partial y} + L_{66} \frac{\partial^2 \phi_x}{\partial y^2} + L_{12} \frac{\partial^2 \phi_y}{\partial x \partial y} \\
& - 2H_{66} \frac{\partial^3 w}{\partial y^2 \partial x} + L_{66} \frac{\partial^2 \phi_y}{\partial x \partial y} + F_{11} \frac{\partial^2 u}{\partial x^2} - I_{13} \frac{\partial^2 u}{\partial t^2} + I_{23} \frac{\partial^3 w}{\partial t^2 \partial x} \\
& - I_{33} \frac{\partial^2 \phi_x}{\partial t^2} - L_{55} \frac{\partial \phi_z}{\partial x} + \tau_{15} \frac{\partial \psi}{\partial x} - L_{55} \phi_x = 0
\end{aligned} \tag{36}$$

$$\begin{aligned}
 \delta\phi_y : & \mu_{32} \frac{\partial \psi}{\partial y} - H_{22} \frac{\partial^3 w}{\partial y^3} + F_{66} \frac{\partial^2 u}{\partial y \partial x} + L_{22} \frac{\partial^2 \phi_y}{\partial y^2} - H_{12} \frac{\partial^3 w}{\partial x^2 \partial y} \\
 & + F_{23} \frac{\partial \phi_z}{\partial y} + F_{66} \frac{\partial^2 v}{\partial x^2} + F_{12} \frac{\partial^2 u}{\partial x \partial y} + L_{66} \frac{\partial^2 \phi_y}{\partial x^2} + F_{22} \frac{\partial^2 v}{\partial y^2} \\
 & + L_{12} \frac{\partial^2 \phi_x}{\partial x \partial y} - 2H_{66} \frac{\partial^3 w}{\partial x^2 \partial y} + L_{66} \frac{\partial^2 \phi_x}{\partial x \partial y} - L_{44} \frac{\partial \phi_z}{\partial y} + \tau_{24} \frac{\partial \psi}{\partial y} \\
 & - L_{44} \phi_y - I_{33} \frac{\partial^2 \phi_y}{\partial t^2} - I_{13} \frac{\partial^2 v}{\partial t^2} + I_{23} \frac{\partial^3 w}{\partial t^2 \partial y} = 0 \\
 \\
 \delta\phi_z : & -\tau_{15} \frac{\partial^2 \psi}{\partial x^2} + L_{55} \frac{\partial \phi_x}{\partial x} + L_{55} \frac{\partial^2 \phi_z}{\partial x^2} + B_{13} \frac{\partial^2 w}{\partial x^2} - F_{13} \frac{\partial \phi_x}{\partial x} \\
 & + B_{23} \frac{\partial^2 w}{\partial y^2} - \tau_{24} \frac{\partial^2 \psi}{\partial y^2} + L_{44} \frac{\partial^2 \phi_z}{\partial y^2} + L_{44} \frac{\partial \phi_y}{\partial y} + B_{13} \frac{\partial^2 w}{\partial x^2} - F_{13} \frac{\partial \phi_x}{\partial x} \\
 & + B_{23} \frac{\partial^2 w}{\partial y^2} - A_{33} \phi_z - \zeta_{33} \psi - F_{23} \frac{\partial \phi_y}{\partial y} - A_{13} \frac{\partial u}{\partial x} - A_{23} \frac{\partial v}{\partial y} \\
 & - J_{21} \frac{\partial^2 w}{\partial t^2} - J_{22} \frac{\partial^2 \phi_z}{\partial t^2} = 0 \\
 \\
 \delta\psi : & \tau_{15} \frac{\partial \phi_x}{\partial x} + \tau_{15} \frac{\partial^2 \phi_z}{\partial x^2} + \Xi_{11} \frac{\partial^2 \psi}{\partial x^2} + \tau_{24} \frac{\partial \phi_y}{\partial y} + \tau_{24} \frac{\partial^2 \phi_z}{\partial y^2} \\
 & + \Xi_{22} \frac{\partial^2 \psi}{\partial y^2} - \Xi_{33} \psi + \mu_{31} \frac{\partial \phi_x}{\partial x} + \mu_{32} \frac{\partial \phi_y}{\partial y} - I_{31} \frac{\partial^2 w}{\partial x^2} - I_{32} \frac{\partial^2 w}{\partial y^2} \\
 & + \zeta_{33} \phi_z + \zeta_{31} \frac{\partial u}{\partial x} + \zeta_{32} \frac{\partial v}{\partial y} = 0
 \end{aligned}$$

It should be noted that three assumptions have been considered in the derivation of equation of motion of the sandwich plate, namely (a) all layers have the same transverse displacement, (b) no slippage occurs between adjacent layers and (c) considering the equivalent single-layer method.

#### 4. Solution procedure

For a plate with simple supports, the following solution can be considered based on Navier's solution:

$$\begin{aligned}
u(x, y, t) &= \sum_{m=1}^{\infty} \sum_{n=1}^{\infty} U_{mn} \cos\left(\frac{m\pi}{a}x\right) \sin\left(\frac{n\pi}{b}y\right) e^{i\omega t} \\
v(x, y, t) &= \sum_{m=1}^{\infty} \sum_{n=1}^{\infty} V_{mn} \cos\left(\frac{m\pi}{a}x\right) \sin\left(\frac{n\pi}{b}y\right) e^{i\omega t} \\
w(x, y, t) &= \sum_{m=1}^{\infty} \sum_{n=1}^{\infty} W_{mn} \cos\left(\frac{m\pi}{a}x\right) \sin\left(\frac{n\pi}{b}y\right) e^{i\omega t} \\
\phi_x(x, y, t) &= \sum_{m=1}^{\infty} \sum_{n=1}^{\infty} X_{mn} \cos\left(\frac{m\pi}{a}x\right) \sin\left(\frac{n\pi}{b}y\right) e^{i\omega t} \\
\phi_y(x, y, t) &= \sum_{m=1}^{\infty} \sum_{n=1}^{\infty} Y_{mn} \cos\left(\frac{m\pi}{a}x\right) \sin\left(\frac{n\pi}{b}y\right) e^{i\omega t} \\
\phi_z(x, y, t) &= \sum_{m=1}^{\infty} \sum_{n=1}^{\infty} Z_{mn} \cos\left(\frac{m\pi}{a}x\right) \sin\left(\frac{n\pi}{b}y\right) e^{i\omega t} \\
\psi(x, y, t) &= \sum_{m=1}^{\infty} \sum_{n=1}^{\infty} \Psi_{mn} \cos\left(\frac{m\pi}{a}x\right) \sin\left(\frac{n\pi}{b}y\right) e^{i\omega t}
\end{aligned} \tag{37}$$

Substituting Eq. (37) into Eq. (36) leads to the following eigenvalue equation:

$$\left( [K] + \omega [C] + \omega^2 [M] \right) \begin{Bmatrix} U_{mn} \\ V_{mn} \\ W_{mn} \\ X_{mn} \\ Y_{mn} \\ Z_{mn} \\ \Psi_{mn} \end{Bmatrix} = \{0\} \tag{38}$$

In which, [K], [M] and [C] are symmetric matrices presented by details in Appendix C. By solving the eigenvalue equation (36), the natural frequencies of the 5-layer sandwich plate can be achieved for different values of mode numbers such as m and n. The Navier analytical method gives closed-form solutions for the linear problem which is easy to implement and exact, however, it is not suitable for nonlinear problems or more complex geometries.

## 5. Numerical results

In this section, numerical results are reported for the analytical solution presented previously. For the sake of validation, consider a single layer homogeneous square plate of  $a/h=10$  and  $\nu=0.3$  with no foundation ( $K_w=0$ ,  $K_G=0$ ). For different values of mode numbers m and n, nondimensional natural frequency of the plate ( $\lambda=\omega h(\rho/G)^{0.5}$ ) are presented in Table 1 against corresponding ones reported by other authors [62, 63]. As shown in this table, results with high accuracy can be obtained.

**Table 1. Dimensionless natural frequencies ( $\lambda=\omega h(\rho/G)^{0.5}$ ) of a single layer, homogeneous square plate ( $a/h=10$ ,  $\nu=0.3$ ,  $K_w=0$ ,  $K_G=0$ )**

(m,n)	Present	Exact 3D solution [62]	HSDT [63]
(1,1)	0.0933	0.0932	0.0931
(1,2)	0.2230	0.2226	0.2222
(2,2)	0.3428	0.3421	0.3411
(1,3)	0.4182	0.4171	0.4158
(2,3)	0.5253	0.5239	0.5221

(3,3)	0.6911	0.6889	0.6862
(2,4)	0.7537	0.7511	0.7481
(1,5)	0.9304	0.9268	0.9230
(4,4)	1.0938	1.0889	1.0847
Maximum Error (%)	-	0.45	0.83

Again, a single layer homogeneous rectangular plate of  $a/b=0.5$ ,  $a/h=10$  and  $\nu=0.3$  with no foundation ( $K_w=0$ ,  $K_G=0$ ) is selected. Table 2 shows dimensionless values of the natural frequency of the plate ( $\Omega=\omega a^2(\rho/E)^{0.5}/h$ ) for various values of mode number  $m$  and  $n$  along with the corresponding values predicted by Hebali et al. [64]. As shown in this table, the results are in high agreement.

**Table 2. Dimensionless natural frequencies ( $\Omega=\omega a^2(\rho/E)^{0.5}/h$ ) of a single layer homogeneous rectangular plate ( $a/b=0.5$ ,  $a/h=10$ ,  $\nu=0.3$ ,  $K_w=0$ ,  $K_G=0$ )**

(m,n)	Present	Quasi-3D [64]
(1,1)	3.70480	3.69590
(1,2)	5.85420	5.83920
(2,2)	13.9760	13.9324
(2,3)	17.1641	17.1070
(3,2)	26.1598	26.0579
(3,3)	28.9933	28.8754
Maximum Error (%)	-	0.79

Consider a thin square plate of  $b/h=300$  and  $\nu=0.3$  with no foundation ( $K_w=0$ ,  $K_G=0$ ). Values of the first three natural frequencies are presented in Table 3 in a dimensionless form ( $\Lambda=\omega a^2(\rho h/D)^{0.5}$ ,  $D=Eh^3/12(1-\nu^2)$ ) against corresponding ones reported by other authors [65-68]. This table confirms the high accuracy of the presented solution and the achieved results.

**Table 3. Dimensionless natural frequencies ( $\Lambda=\omega a^2(\rho h/D)^{0.5}$ ,  $D=Eh^3/12(1-\nu^2)$ ) of a single layer, homogeneous square plate ( $b/h=300$ ,**

**$\nu=0.3$ ,  $K_w=0$ ,  $K_G=0$ )**

	Mode 1	Mode 2	Mode 3	Maximum Error (%)
Present work	19.7899	49.4718	98.9337	-
Exact solution [66]	19.7392	49.3480	98.6960	0.25
Finite element method [67]	19.7392	49.3480	98.7162	0.25
Differential quadrature method [68]	19.7392	49.3453	98.6268	0.31
Galerkin method [65]	19.7362	49.3431	98.6765	0.27

An isotropic homogeneous single layer square plate of  $\nu=0.3$  resting on an elastic foundation is considered. For different values of thickness to length ratio ( $h/a$ ) and nondimensional Winkler and shear coefficients of the foundation ( $\hat{K}_w = K_w a^4/D$ ,  $\hat{K}_G = K_G a^2/D$ ,  $D=Eh^3/12(1-\nu^2)$ ), natural frequencies of the plate are presented in Table 4 in a dimensionless form ( $\Lambda=\omega a^2(\rho h/D)^{0.5}$ ) against corresponding ones reported by other authors [69-71]. The results of this table confirm the accuracy of the presented solution.

**Table 4. Dimensionless natural frequencies ( $\Lambda=\omega a^2(\rho h/D)^{0.5}$ ,  $D=Eh^3/12(1-\nu^2)$ ) of a single layer, homogeneous square plate ( $\nu=0.3$ )**

$\frac{h}{a}$	$\hat{K}_w, \hat{K}_G$	Akhavan et al. [69]	Atmane et al. [70]	Moradi et al. [71]	Present
0.001	(0,0)	19.7391	19.7392	19.7396	19.7904
	(100,10)	26.2112	26.2112	26.2115	26.2499
	(1000,100)	57.9961	57.9962	57.9963	58.0136
0.1	(0,0)	19.0840	19.0658	19.0658	19.1196
	(100,10)	25.6368	25.6236	25.6235	25.5733
	(1000,100)	57.3969	57.3923	57.3922	56.9680
0.2	(0,0)	17.5055	17.4531	17.4530	17.5141
	(100,10)	24.3074	24.2728	24.2728	23.9892
	(1000,100)	56.0359	56.0311	56.0363	56.0145

After validation of the applied method, vibration behaviors of the square power-law FGM sandwich plates with four simply supported edges are investigated. The top and bottom layers are considered homogeneous plates and made of aluminium ( $E_m=70Gp$ ,  $\rho_m=2707Kg/m^3$ ) and alumina ( $E_c=380Gp$ ,  $\rho_c=3800Kg/m^3$ ), respectively. The effective material properties of FGM core, like Young’s modulus and mass density, then can be expressed by the rule of mixture[72] as  $\xi_{core}(z) = (\xi_m - \xi_c)((2z + h_c) / 2h_c)^k + \xi_c$ .

Table 5. Reports Fundamental normalized frequency parameters (for  $n=1$  and  $m=1$ ) of power-law FGM sandwich square plates ( $a/b=1$ ) with Three thickness-side ratios  $h/b$  (0.01, 0.1, 0.2) and four-volume fraction indices  $k$  (0.5,1,5,10). As observed, increasing the ratio of  $h/b$  reduces all the frequency parameters of the sandwich square plates, also increasing of the volume fraction indices  $k$ , increases the frequencies.

**Table 5. Fundamental frequency parameters ( $(\Omega=\omega b^2(\rho_0/E_0)^{0.5}/(h_{core}+h_c+h_m))$ , ( $\rho_0=1Kg/m^3$ ,  $E_0=1GPa$ )) of simply supported square 1-8-1 power-law FGM sandwich plates with FGM core ( $h_{core}/h_m=8$ ,  $h_c/h_m=1$ ,  $\nu=0.3$ ,  $K_w=0$ ,  $K_G=0$ )**

$\frac{h}{b}$	$k$	Q. le et al.[72]	Present
0.01	0.5	1.33931	1.3713
	1	1.38669	1.4179
	5	1.53143	1.5470
	10	1.59105	1.6014
0.1	0.5	1.29751	1.3273
	1	1.34847	1.3777
	5	1.49309	1.5080
	10	1.54980	1.5600
0.2	0.5	1.19580	1.2210
	1	1.25338	1.2783
	5	1.39567	1.4094
	10	1.44540	1.4557

What follows, numerical examples are presented to study the influences of various parameters on the natural frequencies of the 5-layer sandwich plates. Except for the cases which are mentioned directly, mechanical properties

are considered as those mentioned in Table 6. Porosity distribution is considered as asymmetric with porosity parameter  $e_1=0.6$ , Skempton coefficient  $B=0.5$  and CNTs are distributed with total volume fraction  $V_r^*=0.11$  based on uniform distribution pattern. Elastic and shear stiffness coefficients of the foundation are selected as  $K_w=10^9$  N/m<sup>3</sup> and  $K_G=10^5$  N/m and the following dimensionless definition is defined as the first natural frequency:

$$\tilde{\omega} = \omega h \sqrt{\frac{2(1+\nu)\rho_1}{E_1}} \tag{39}$$

**Table 6. Mechanical properties**

Core [9] (Tennessee marble)	Interior layers		Piezoelectric face sheets [73]		
	Matrix [71] (Methyl-methacrylate)	Reinforcement [74] CNT (R=10 A°)			
$E_1=60$ GPa $\nu=0.25$ $\rho_1=2700$ kg/m <sup>3</sup> $\alpha=0.19$	$E=2.5$ GPa $\nu=0.34$ $\rho=1150$ kg/m <sup>3</sup>	$k_r=30$ GPa $l_r=10$ GPa $m_r=1$ GPa $n_r=450$ GPa $p_r=1$ GPa $\rho_r=1400$ kg/m <sup>3</sup>	$C_{11}^p = 226$ GPa $C_{12}^p = 125$ GPa $C_{13}^p = 124$ GPa $C_{22}^p = 226$ GPa $C_{33}^p = 216$ GPa $C_{44}^p = 44.2$ GPa $C_{55}^p = 44.2$ GPa $C_{66}^p = 50.5$ GPa $\rho = 5550$ Kg/m <sup>3</sup>	$e_{31}=e_{32}=-2.2$ C/m <sup>2</sup> $e_{15}=e_{24}=5.8$ C/m <sup>2</sup> $e_{33}=9.3$ C/m <sup>2</sup>	$k_{11}=5.64 \times 10^9$ C/Vm $k_{22}=5.64 \times 10^9$ C/Vm $k_{33}=6.35 \times 10^9$ C/Vm

The square sandwich structure with  $h/h_p=6$  and constant surface area ( $S=a.b$ ) is shown in Figures 3, 4, and 5 for three types of nonsymmetric, symmetric, and monotonous pore distribution, and it is included to study the effect of natural frequency variations based on the porous core thickness to nanocomposite layer thickness ratio  $h_c/h_{nc}$  for different porosity values. The figures show that for all 3 distribution types, by increasing the porosity parameter which means that with an increase in the size of pores, the natural frequencies of the sandwich plate increase, because by increasing the porosity, the mass, and structural stiffness both decrease, but all three figures show that the mass reduction of the structure is much larger than the stiffness reduction for a given layer thickness, which leads to the increased natural frequency.

In addition, to understand the effect of geometric parameters such as the layer thickness, as shown in the figures, by increasing the ratio of the porous core thickness to the nanocomposite for nonsymmetric and symmetric distributions shown in Figure 3 and 4 respectively in the interval  $[0,0.7]$  and for monotonous distribution in the interval  $[0,0.5]$  as shown in Figure 5, due to the reduction of the structural stiffness, the natural frequencies are attenuated and for higher porosities in these intervals, the trends are reversed. Consequently, if the goal is to increase the natural frequency of a structure, the optimum situation can be found by selecting the porosity distribution for a specified layer thickness and changing the porosity value.

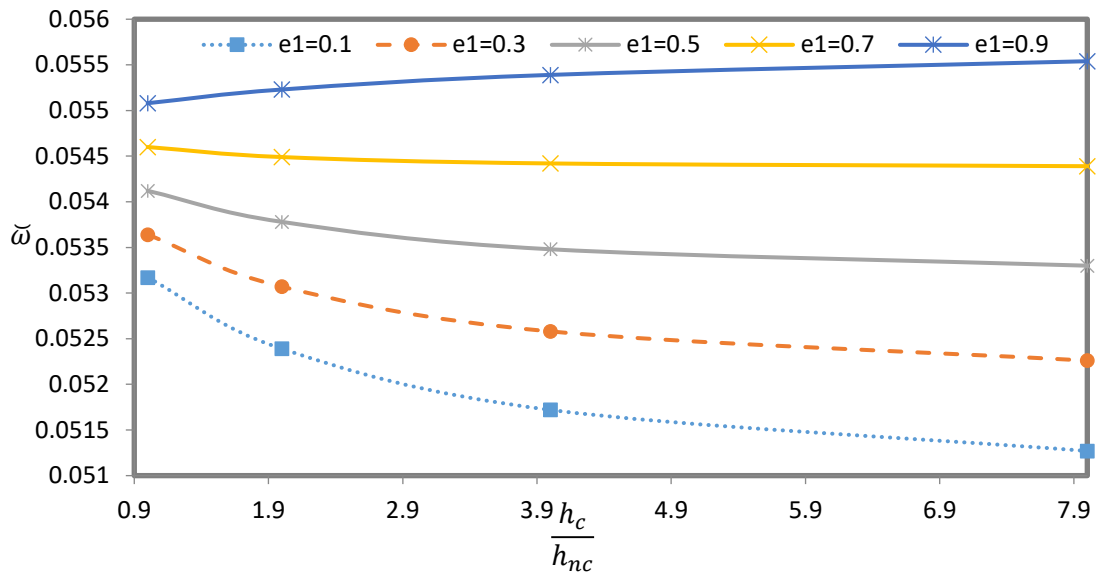


Figure 3. The dimensionless natural frequency of sandwich plate versus layer thickness ratio ( $h_c/h_{nc}$ ) for various values of porosity parameter of nonsymmetric distribution pattern.

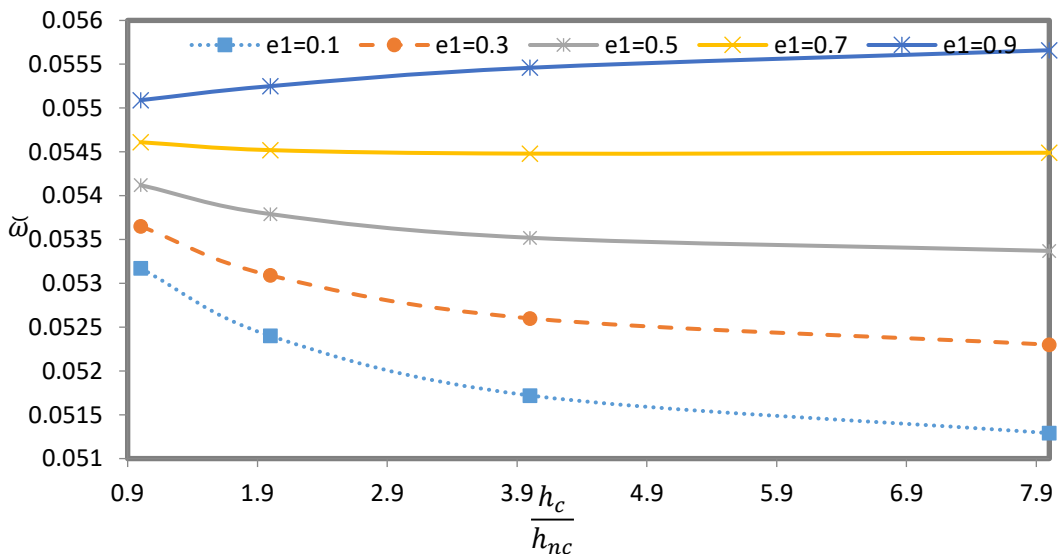


Figure 4. The dimensionless natural frequency of sandwich plate versus layer thickness ratio ( $h_c/h_{nc}$ ) for various values of porosity parameter of symmetric distribution pattern.

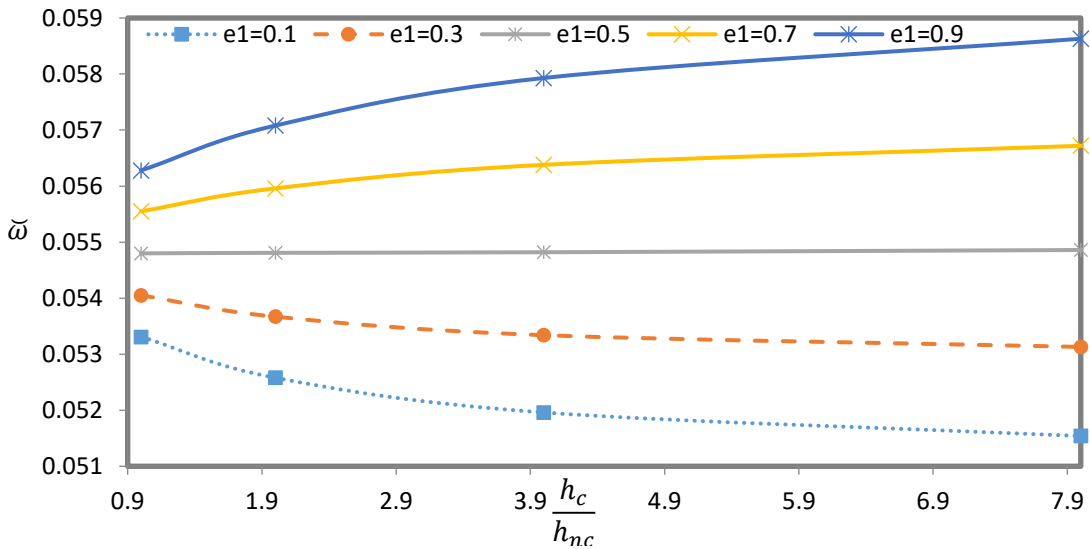


Figure 5. The dimensionless natural frequency of sandwich plate versus layer thickness ratio ( $h_c/h_{nc}$ ) for various values of porosity parameter of monotonous distribution pattern.

Figure 6 shows the comparison of various distributions for a given value of porosity parameter  $e_1=0.4$  for a square sandwich plate with a constant surface area of ( $S=a.b$ ) at  $h/h_p=6$ . As shown in this figure, the natural frequencies for all 3 distribution models decrease by increasing the layer thickness ratio, but for all layer thickness ratios, the fundamental frequency of the monotonous distribution model is greater than the symmetric and nonsymmetric distribution models with a large margin, which could be caused by a higher increase in mass and stronger improvement of stiffness in the monotonous distribution case compared with the symmetric and nonsymmetric distributions for a given porosity value. The values of natural frequency in the symmetric and asymmetric cases are similar which is because the stiffness to mass ratio of the structure is similar in the functional behavior of the two porous distributions, but as shown in the figure, increasing the core thickness while keeping the total thickness constant, results in a greater reduction in the frequency for the asymmetric case compared with the symmetric case.

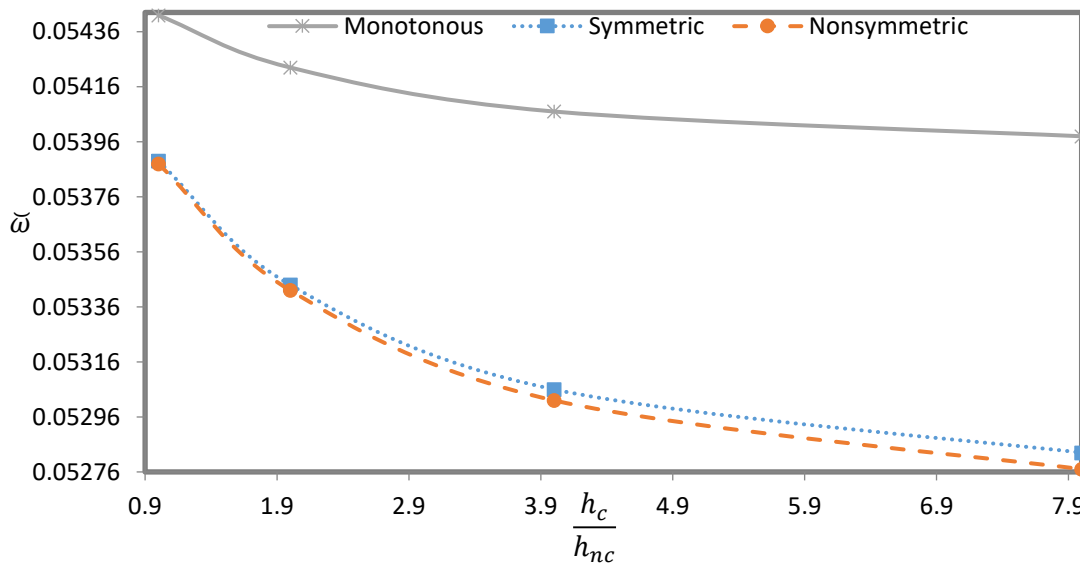


Figure 6. The dimensionless natural frequency of sandwich plate versus layer thickness ratio ( $h_c/h_{nc}$ ) for different distribution patterns.

The effect of porosity coefficient ( $0 < e_1 < 0.95$ ), porosity distribution model, and layer thickness  $h_c/h_{nc}=10$  and  $h_p/h_{nc}=1$ , on frequency modes For different values of mode numbers  $m$  and  $n$ , ( $\bar{\omega}_{mn}, \bar{\omega}_{11}, \bar{\omega}_{12}, \bar{\omega}_{22}$ ) is studied in Figures 7, 8, and 9. As shown in Figures 7 and 8, only for nonsymmetric and symmetric cases, by increasing the porosity

parameter, the fundamental frequencies ( $\tilde{\omega}_{11}$ ) always increase, and in other cases, based on the porosity distribution and the frequency mode number, it increases first and then decreases. The maximum frequency in different modes could be an significant design factor that is shown based on the type of the porosity distribution.

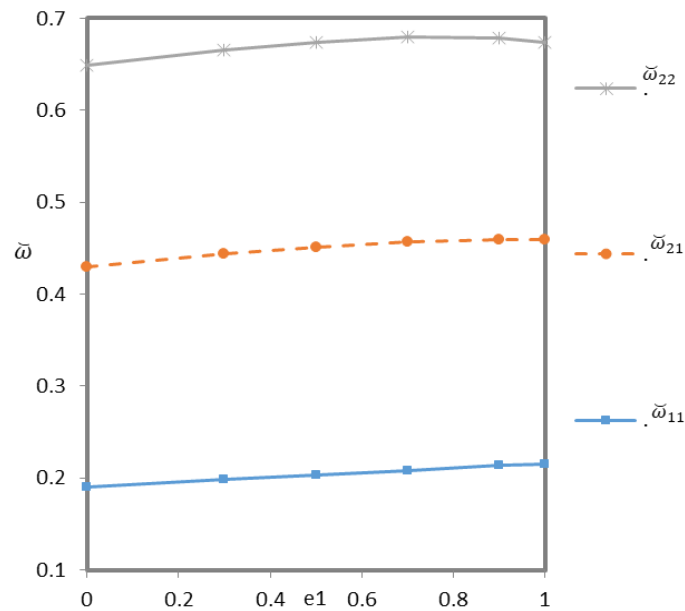


Figure 7. The dimensionless natural frequency of sandwich plate versus porosity parameter for nonsymmetric distribution pattern.

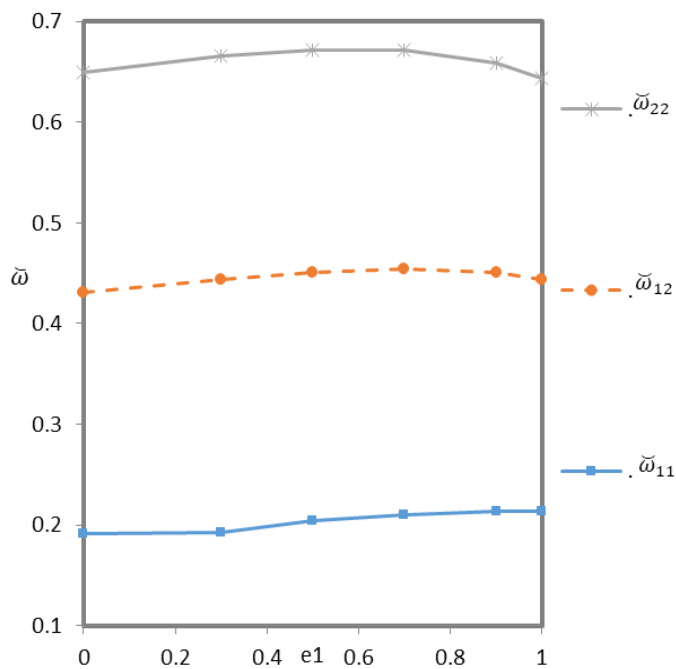


Figure 8. The dimensionless natural frequency of sandwich plate versus porosity parameter for symmetric distribution pattern.

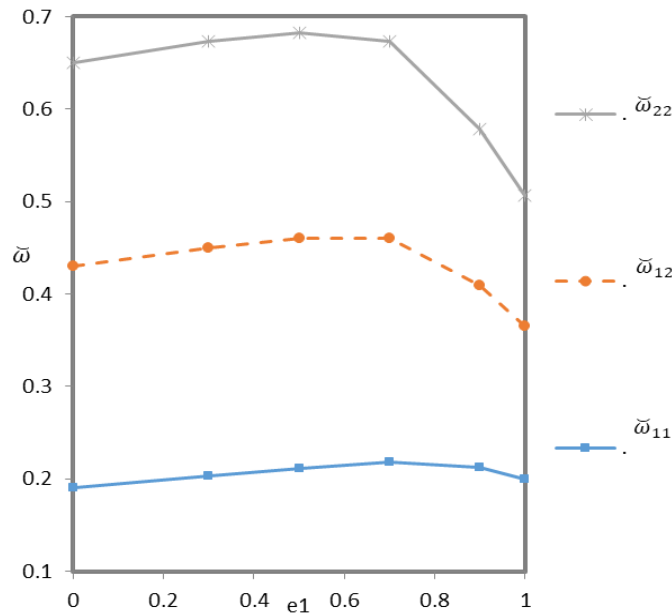


Figure 9. The dimensionless natural frequency of sandwich plate versus porosity parameter for monotonous distribution pattern.

Figure 10 shows the fundamental natural frequency variations based on aspect ratio ( $a/b$ ) of a sandwich plate  $h_c/h_{nc}=10$  and  $h_p/h_{nc}=1$  with constant surface area ( $s=a.b$ ) and fixed volume ( $V=s.h$ ) for two values of Skempton coefficient. As shown in this figure, the minimum values of the natural frequencies belong to a square plate ( $a/b=1$ ). For  $a/b<1$  an increase in the value of aspect ratio decreases all-natural frequencies and for  $a/b>1$  reverse trend can be seen. Also, by increasing the Skempton factor, the fundamental natural frequency in all 3 cases of porosity distribution increases. So that by increasing the Skempton factor, the pore compression increases, and the stiffness increase is higher than the mass increase, leading to higher natural frequencies. The natural frequencies are at their maximum value for monotonous distribution and  $B=0.8$  and at their minimum for nonsymmetric distribution and  $B=0$ .

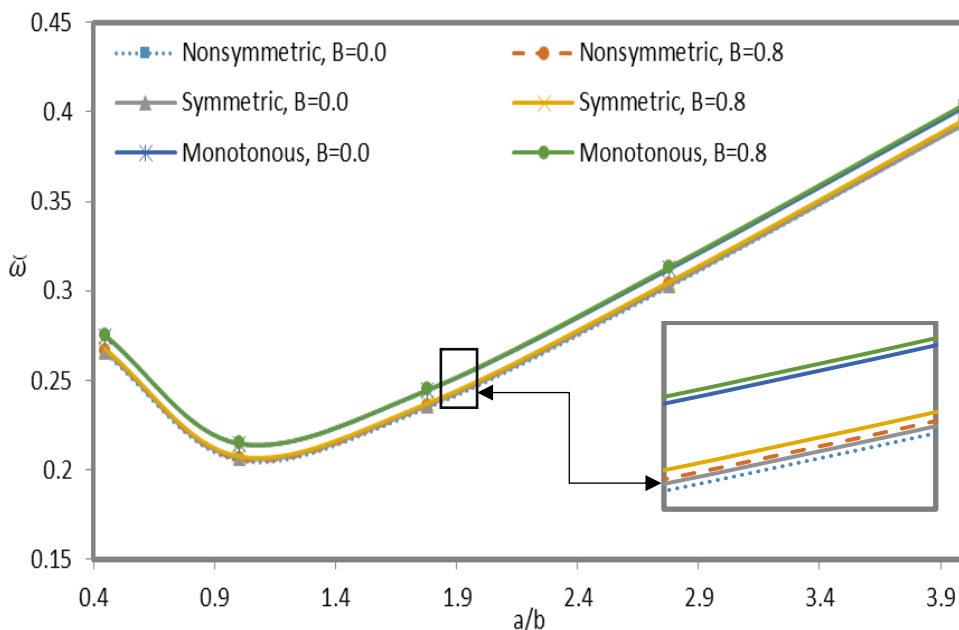
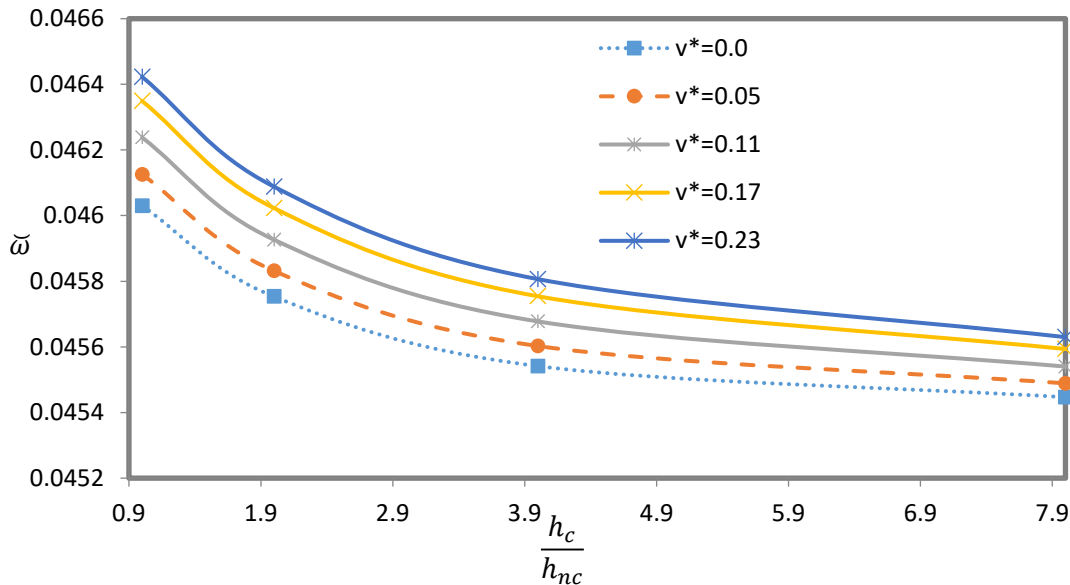


Figure 10. The dimensionless natural frequency of sandwich plate versus aspect ratio ( $a/b$ ) for different distribution patterns and Skempton coefficients.

Figure 11 shows the influence of the total volume fraction of CNTs on the natural frequencies of the sandwich square plate of  $h/h_p=6$ . This figure confirms that all-natural frequencies increase with the rise in the value of the total volume fraction of CNTs which can be explained by an increase in the flexural rigidity of the CNT-reinforced interior layers. In other words, as the volume fraction of CNTs in Eq. (20) becomes greater,  $G_{nc}$  and  $K_{nc}$  that are shear and bulk moduli of the CNT-reinforced layers respectively will increase. Therefore, according to Eq. (19), the mechanical properties of nanocomposite layers increase. So the stiffness of the sandwich plate enhances which leads the natural frequency to increase. This result is in complete agreement with [75],[71] and [76].



**Figure 11. The dimensionless natural frequency of sandwich plate versus layer thickness ratio ( $h_c/h_{nc}$ ) for various volume fraction of CNTs.**

The variations in the natural frequency of the sandwich structure ( $h_c/h_{nc}=1$  and  $h_p/h_{nc}=1$ ) based on aspect ratio ( $a/b$ ) for the various elastic medium models, Winkler and shear coefficients of the foundation and damper modulus parameter are shown in Figure 12. As shown, when the Pasternak model is used for the elastic medium, the natural frequency compared to other models is at its maximum. This is due to the Winkler constant and shear layer in this model which has an increasing effect on the natural frequencies. As expected, the frequency vs. aspect ratio curve for the Visco-Pasternak model is lower than Winkler and Pasternak models due to the presence of damping constant in addition to the Winkler constant and the shear layer.

As these figures show, an increase in both Winkler and shear coefficients of the foundation, all-natural frequencies grow which can be explained by the increase in the value of stiffness of the plate-foundation system but viscoelastic behavior leads to energy damping and force dissipation, and by increasing the damper modulus parameter, the frequency experiences a higher decrease due to the system damping effect.

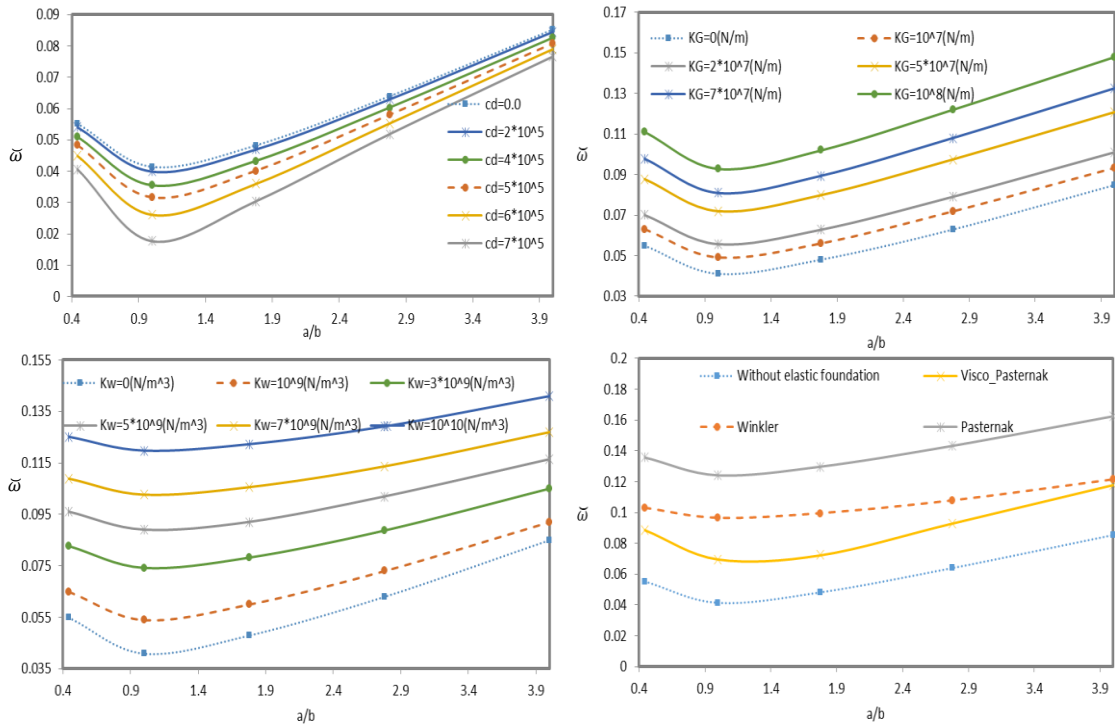


Figure 12. The dimensionless natural frequency of sandwich plate versus aspect ratio(a/b) for different damping coefficients, foundations, Winkler and shear layer constants

The natural frequency variations of the square sandwich plate with  $h/h_c=6$ , are shown in Figure 13 based on the layer thickness ratio under applied external voltage. As shown, when the applied voltage changes from negative to positive, the natural frequency decreases. The sandwich plate sensitivity to applied positive and negative voltages is due to the tensile and compressive forces since the tensile forces weaken the stiffness and compressive forces enhance the stiffness; consequently, the effects result in softening and hardening of the structure which leads to a decrease and increase of the structural natural frequency, respectively. As a result, the applied external voltage value could be an effective parameter for controlling the vibration of sandwich structure.

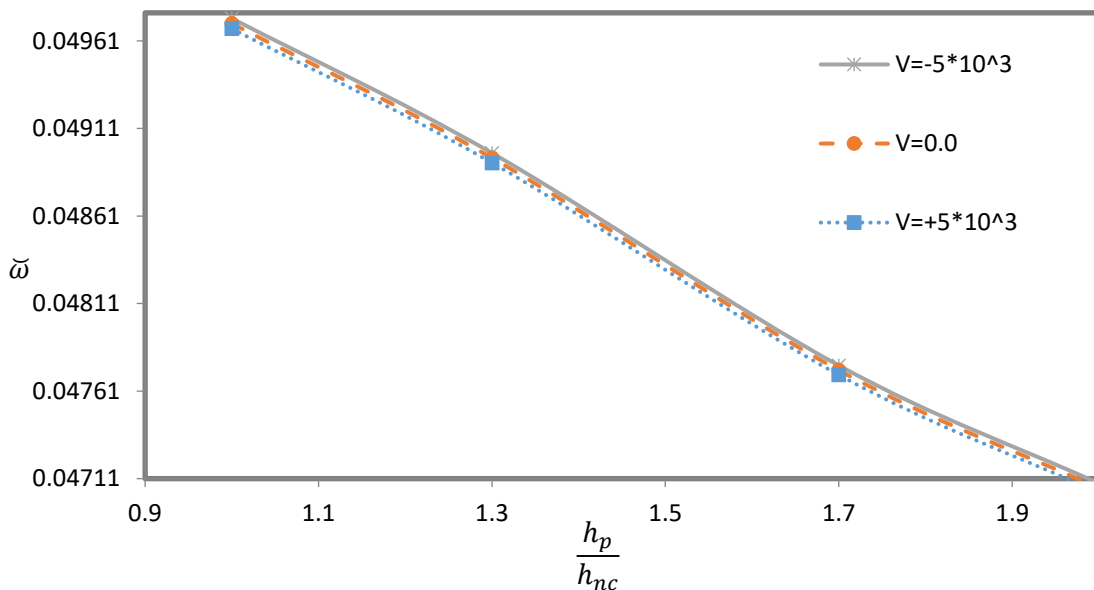


Figure 13. The dimensionless natural frequency of sandwich plate versus layer thickness ratio ( $h_p/h_{nc}$ ) for various values of external voltage.

## 6. Conclusions

Using Navier's method, an exact solution was presented for free vibration characteristics of 5-layer sandwich plates consisting of a sutured porous material core, CNT-reinforced interior layers and piezoelectric face sheets that are subjected to an external electric voltage. The plate was modelled using the quasi-3D sinusoidal shear deformation theory and the set of the governing equations are derived using Hamilton's principle. The accuracy of the presented solution was validated and the influence of various parameters on the natural frequencies of the sandwich plate was investigated. The objectives of this study include optimum application of new and smart materials. Using a porous core for reducing structural weight, improving flexibility and reducing cost also affects the structural strength. Composites reinforced with carbon nanotubes enhance structural strength, while adding piezoelectric functional layers can turn the material into a smart structure, which are widely used in sandwich panel structures such as applications in aerospace and airplane wings.

Numerical examples showed that:

- the natural frequency increases with increasing the value of the porosity parameter. Also by an optimum selection of porosity parameter and porosity distribution, the frequency reduction can be reversed which occurs by increasing the layer thickness ratio.
- the minimum values of the natural belong to a square plate ( $a/b=1$ ). In addition to a given optimum porosity percentage for a sandwich plate for constant volume and area, the maximum increase in natural frequency occurs.
- the monotonous case had the highest natural frequencies and the least amount is for the nonsymmetric case.
- all-natural frequencies increase with increasing the value of the total volume fraction of CNTs.
- by increasing Winkler modulus and shear modulus of the surrounding elastic medium, natural frequent increases but by increasing damper modulus parameter, natural frequencies decrease.
- The medium effect on natural frequency follows the order Pasternak medium > Winkler medium > Visco-Pasternak medium > Without elastic medium.
- By changing the externally applied voltage to piezoelectric overlays from positive to negative, the natural frequency can be increased. It should be noted that
- For optimum use of piezoelectric materials, instead of a continuous layer, piezoelectric patches can be used.

## Appendix A

$$\begin{aligned}
 \{I_{11}, I_{12}, I_{13}, I_{22}, I_{23}, I_{33}, J_{21}, J_{22}\} &= \int_{-\frac{h}{2}}^{\frac{h_c}{2}-h_{nc}} \rho_p \left\{ 1, z, f, z^2, zf, f^2, \frac{df}{dz}, \left(\frac{df}{dz}\right)^2 \right\} dz + \\
 &\int_{-\frac{h_c}{2}-h_{nc}}^{\frac{h_c}{2}} \rho_{nc} \left\{ 1, z, f, z^2, zf, f^2, \frac{df}{dz}, \left(\frac{df}{dz}\right)^2 \right\} dz + \int_{-\frac{h_c}{2}}^{\frac{h_c}{2}} \rho_e \left\{ 1, z, f, z^2, zf, f^2, \frac{df}{dz}, \left(\frac{df}{dz}\right)^2 \right\} dz + \\
 &\int_{\frac{h_c}{2}}^{\frac{h_c}{2}+h_{nc}} \rho_{nc} \left\{ 1, z, f, z^2, zf, f^2, \frac{df}{dz}, \left(\frac{df}{dz}\right)^2 \right\} dz + \int_{\frac{h_c}{2}+h_{nc}}^{\frac{h}{2}} \rho_p \left\{ 1, z, f, z^2, zf, f^2, \frac{df}{dz}, \left(\frac{df}{dz}\right)^2 \right\} dz
 \end{aligned} \tag{A-1}$$

Appendix B

$$\{A_{ij}, B_{ij}, F_{ij}, D_{ij}, H_{ij}, L_{ij}\} = \int_{-\frac{h}{2}}^{\frac{h_c-h_{nc}}{2}} C_{ij}^p \{1, z, f, z^2, zf, f^2\} dz + \int_{-\frac{h_c-h_{nc}}{2}}^{\frac{h_c}{2}} C_{ij}^{nc} \{1, z, f, z^2, zf, f^2\} dz + \int_{-\frac{h_c}{2}}^{\frac{h_c}{2}} C_{ij}^c \{1, z, f, z^2, zf, f^2\} dz + \int_{\frac{h_c}{2}}^{\frac{h_c+h_{nc}}{2}} C_{ij}^{nc} \{1, z, f, z^2, zf, f^2\} dz + \int_{\frac{h_c+h_{nc}}{2}}^{\frac{h}{2}} C_{ij}^p \{1, z, f, z^2, zf, f^2\} dz$$

$i, j = 1, 2$

$$\{A_{ii}, B_{ii}, D_{ii}, F_{ii}, H_{ii}, L_{ii}\} = \int_{-\frac{h}{2}}^{\frac{h_c-h_{nc}}{2}} C_{44}^p \left\{1, z, z^2, \frac{df}{dz}, z \frac{df}{dz}, \left(\frac{df}{dz}\right)^2\right\} dz + \int_{-\frac{h_c-h_{nc}}{2}}^{\frac{h_c}{2}} C_{44}^{nc} \left\{1, z, z^2, \frac{df}{dz}, z \frac{df}{dz}, \left(\frac{df}{dz}\right)^2\right\} dz + \int_{-\frac{h_c}{2}}^{\frac{h_c}{2}} C_{44}^c \left\{1, z, z^2, \frac{df}{dz}, z \frac{df}{dz}, \left(\frac{df}{dz}\right)^2\right\} dz + \int_{\frac{h_c}{2}}^{\frac{h_c+h_{nc}}{2}} C_{44}^{nc} \left\{1, z, z^2, \frac{df}{dz}, z \frac{df}{dz}, \left(\frac{df}{dz}\right)^2\right\} dz + \int_{\frac{h_c+h_{nc}}{2}}^{\frac{h}{2}} C_{44}^p \left\{1, z, z^2, \frac{df}{dz}, z \frac{df}{dz}, \left(\frac{df}{dz}\right)^2\right\} dz$$

$i = 4, 5$

(B-1)

$$\{A_{66}, B_{66}, D_{66}, F_{66}, H_{66}, L_{66}\} = \int_{-\frac{h}{2}}^{\frac{h_c-h_{nc}}{2}} C_{66}^p \{1, 2z, 2z^2, f, zf, f^2\} dz + \int_{-\frac{h_c-h_{nc}}{2}}^{\frac{h_c}{2}} C_{66}^{nc} \{1, 4z, 4z^2, f, zf, f^2\} dz + \int_{-\frac{h_c}{2}}^{\frac{h_c}{2}} C_{66}^c \{1, 2z, 2z^2, f, zf, f^2\} dz + \int_{\frac{h_c}{2}}^{\frac{h_c+h_{nc}}{2}} C_{66}^{nc} \{1, 4z, 4z^2, f, zf, f^2\} dz + \int_{\frac{h_c+h_{nc}}{2}}^{\frac{h}{2}} C_{66}^p \{1, 2z, 2z^2, f, zf, f^2\} dz$$

$$\{A_{i3}, B_{i3}, F_{i3}\} = \int_{-\frac{h}{2}}^{\frac{h_c-h_{nc}}{2}} C_{i3}^p \left\{\frac{d^2f}{dz^2}, z \frac{d^2f}{dz^2}, f \frac{d^2f}{dz^2}\right\} dz + \int_{-\frac{h_c-h_{nc}}{2}}^{\frac{h_c}{2}} C_{i3}^{nc} \left\{\frac{d^2f}{dz^2}, z \frac{d^2f}{dz^2}, f \frac{d^2f}{dz^2}\right\} dz + \int_{-\frac{h_c}{2}}^{\frac{h_c}{2}} C_{i3}^c \left\{\frac{d^2f}{dz^2}, z \frac{d^2f}{dz^2}, f \frac{d^2f}{dz^2}\right\} dz + \int_{\frac{h_c}{2}}^{\frac{h_c+h_{nc}}{2}} C_{i3}^{nc} \left\{\frac{d^2f}{dz^2}, z \frac{d^2f}{dz^2}, f \frac{d^2f}{dz^2}\right\} dz + \int_{\frac{h_c+h_{nc}}{2}}^{\frac{h}{2}} C_{i3}^p \left\{\frac{d^2f}{dz^2}, z \frac{d^2f}{dz^2}, f \frac{d^2f}{dz^2}\right\} dz \quad i = 1, 2$$

$$\begin{aligned}
A_{33} &= \int_{-\frac{h}{2}}^{\frac{h_c-h_{nc}}{2}} C_{33}^p \left( \frac{d^2 f}{dz^2} \right)^2 dz + \int_{-\frac{h_c-h_{nc}}{2}}^{\frac{h_c}{2}} C_{33}^{nc} \left( \frac{d^2 f}{dz^2} \right)^2 dz + \\
&\int_{-\frac{h_c}{2}}^{\frac{h_c}{2}} C_{33}^c \left( \frac{d^2 f}{dz^2} \right)^2 dz + \int_{\frac{h_c}{2}}^{\frac{h_c+h_{nc}}{2}} C_{33}^{nc} \left( \frac{d^2 f}{dz^2} \right)^2 dz + \int_{\frac{h_c+h_{nc}}{2}}^{\frac{h}{2}} C_{33}^p \left( \frac{d^2 f}{dz^2} \right)^2 dz \\
\{\mathcal{S}_{3i}, \iota_{3i}, \mu_{3i}\} &= \frac{\pi e_{3i}}{h_p} \left[ \int_{-\frac{h}{2}}^{\frac{h_c-h_{nc}}{2}} \sin \left( \frac{\pi z_b}{h_p} \right) \{1, z, f\} dz + \int_{\frac{h_c+h_{nc}}{2}}^{\frac{h}{2}} \sin \left( \frac{\pi z_t}{h_p} \right) \{1, z, f\} dz \right] \quad i=1,2 \\
\mathcal{S}_{33} &= \frac{\pi e_{33}}{h_p} \left[ \int_{-\frac{h}{2}}^{\frac{h_c-h_{nc}}{2}} \sin \left( \frac{\pi z_b}{h_p} \right) \frac{d^2 f}{dz^2} dz + \int_{\frac{h_c+h_{nc}}{2}}^{\frac{h}{2}} \sin \left( \frac{\pi z_t}{h_p} \right) \frac{d^2 f}{dz^2} dz \right] \\
\tau_{ij} &= e_{ij} \left[ \int_{-\frac{h}{2}}^{\frac{h_c-h_{nc}}{2}} \frac{df}{dz} \cos \left( \frac{\pi z_b}{h_p} \right) dz + \int_{\frac{h_c+h_{nc}}{2}}^{\frac{h}{2}} \frac{df}{dz} \cos \left( \frac{\pi z_t}{h_p} \right) dz \right] \quad ij=15,24 \\
\Xi_{ii} &= k_{ii} \left[ \int_{-\frac{h}{2}}^{\frac{h_c-h_{nc}}{2}} \cos^2 \left( \frac{\pi z_b}{h_p} \right) dz + \int_{\frac{h_c+h_{nc}}{2}}^{\frac{h}{2}} \cos^2 \left( \frac{\pi z_t}{h_p} \right) dz \right] \quad i=1,2 \\
\Xi_{33} &= k_{33} \left( \frac{\pi}{h_p} \right)^2 \left[ \int_{-\frac{h}{2}}^{\frac{h_c-h_{nc}}{2}} \sin^2 \left( \frac{\pi z_t}{h_p} \right) dz + \int_{\frac{h_c+h_{nc}}{2}}^{\frac{h}{2}} \sin^2 \left( \frac{\pi z_b}{h_p} \right) dz \right] \\
\Gamma_{31} &= \left[ \int_{-\frac{h}{2}}^{\frac{h_c-h_{nc}}{2}} e_{31} dz + \int_{\frac{h_c}{2}}^{\frac{h}{2}} e_{31} dz \right], \Gamma_{32} = \left[ \int_{-\frac{h}{2}}^{\frac{h_c-h_{nc}}{2}} e_{32} dz + \int_{\frac{h_c}{2}}^{\frac{h}{2}} e_{32} dz \right]
\end{aligned}$$

Appendix C

$$\begin{aligned}
 K_{11} &= -A_{11}\beta_1^2 - A_{66}\beta_2^2 & K_{12} &= -\beta_1\beta_2(A_{12} + A_{66}) & K_{13} &= B_{11}\beta_1^3 + \beta_1\beta_2^2(B_{12} + B_{66}) \\
 K_{14} &= -F_{11}\beta_1^2 - F_{66}\beta_2^2 & K_{15} &= -\beta_1\beta_2(F_{12} + F_{66}) & K_{16} &= A_{13}\beta_1 \\
 K_{17} &= \beta_1\zeta_{31} & K_{22} &= -A_{66}\beta_1^2 - A_{22}\beta_2^2 & K_{23} &= B_{22}\beta_2^3 + \beta_2\beta_1^2(B_{12} + B_{66}) \\
 K_{24} &= -\beta_1\beta_2(F_{12} + F_{66}) & K_{25} &= -F_{66}\beta_1^2 - F_{22}\beta_2^2 & K_{26} &= \beta_2A_{23} & K_{27} &= \beta_2\zeta_{32} \\
 K_{33} &= -2\beta_1^2\beta_2^2(D_{66} + D_{12}) - \beta_1^4D_{11} - \beta_2^4D_{22} - K_W - K_G(\beta_1^2 + \beta_2^2) + \beta_1^2\left(\Gamma_{31}\frac{2V_0}{h_p}\right) + \beta_2^2\left(\Gamma_{32}\frac{2V_0}{h_p}\right) \\
 K_{34} &= H_{11}\beta_1^3 + \beta_1\beta_2^2(H_{12} + 2H_{66}) & K_{35} &= H_{22}\beta_2^3 + \beta_2\beta_1^2(H_{12} + 2H_{66}) & K_{36} &= -B_{13}\beta_1^2 - B_{23}\beta_2^2 \\
 K_{37} &= -\beta_1^2\iota_{31} - \beta_2^2\iota_{32} & K_{44} &= -L_{11}\beta_1^2 - L_{66}\beta_2^2 - L_{55} & K_{45} &= -\beta_1\beta_2(L_{66} + L_{12}) \\
 K_{46} &= \beta_1(F_{13} - L_{55}) & K_{47} &= \beta_1(\mu_{31} + \tau_{15}) & K_{55} &= -L_{22}\beta_2^2 - L_{66}\beta_1^2 - L_{44} \\
 K_{56} &= \beta_2(F_{23} - L_{44}) & K_{57} &= \beta_2(\mu_{32} + \tau_{24}) & K_{66} &= -L_{44}\beta_2^2 - L_{55}\beta_1^2 - A_{33} \\
 K_{67} &= \beta_1^2\tau_{15} + \beta_2^2\tau_{24} - \zeta_{33} & K_{77} &= \Xi_{11}\beta_1^2 + \Xi_{22}\beta_2^2 + \Xi_{33}
 \end{aligned}$$

$$M = \begin{bmatrix} -I_{11} & 0 & \beta_1 I_{12} & -I_{13} & 0 & 0 & 0 \\ & -I_{11} & I_{12}\beta_2 & 0 & -I_{13} & 0 & 0 \\ & & -I_{11} - I_{22}(\beta_1^2 + \beta_2^2) & I_{23}\beta_1 & I_{23}\beta_2 & -J_{21}\omega^2 & 0 \\ & & & -I_{33} & 0 & 0 & 0 \\ & & symmetric & & -I_{33} & 0 & 0 \\ & & & & & -J_{22} & 0 \\ & & & & & & 0 \end{bmatrix}$$

(C.1)

$$C = -iC_d \begin{bmatrix} 0 & 0 & 0 & 0 & 0 & 0 & 0 \\ & 0 & 0 & 0 & 0 & 0 & 0 \\ & & 1 & 0 & 0 & 0 & 0 \\ & & & 0 & 0 & 0 & 0 \\ & & symmetric & & 0 & 0 & 0 \\ & & & & & 0 & 0 \\ & & & & & & 0 \end{bmatrix}$$

where

$$\beta_1 = \frac{m\pi}{a} \quad \beta_2 = \frac{n\pi}{b} \tag{C.2}$$

References

[1] M. Babaei, F. Kiarasi, K. Asemi, M. Hosseini, Functionally graded saturated porous structures: A review, *Journal of Computational Applied Mechanics*, Vol. 53, No. 2, pp. 297-308, 2022.

[2] M. Goodarzi, M. Mohammadi, M. Khooran, F. Saadi, Thermo-Mechanical Vibration Analysis of FG Circular and Annular Nanoplate Based on the Visco-Pasternak Foundation, *Journal of Solid Mechanics*, Vol. 8, No. 4, pp. 788-805, 2016.

- [3] M. Mohammadi, M. Hosseini, M. Shishesaz, A. Hadi, A. Rastgoo, Primary and secondary resonance analysis of porous functionally graded nanobeam resting on a nonlinear foundation subjected to mechanical and electrical loads, *European Journal of Mechanics - A/Solids*, Vol. 77, pp. 103793, 2019/09/01/, 2019.
- [4] M. Mohammadi, A. Rastgoo, Nonlinear vibration analysis of the viscoelastic composite nanoplate with three directionally imperfect porous FG core, *Structural Engineering and Mechanics, An Int'l Journal*, Vol. 69, No. 2, pp. 131-143, 2019.
- [5] M. Mohammadi, A. Rastgoo, Primary and secondary resonance analysis of FG/lipid nanoplate with considering porosity distribution based on a nonlinear elastic medium, *Mechanics of Advanced Materials and Structures*, Vol. 27, No. 20, pp. 1709-1730, 2020/10/15, 2020.
- [6] Y. S. Al Rjoub, A. G. Hamad, Free vibration of functionally Euler-Bernoulli and Timoshenko graded porous beams using the transfer matrix method, *KSCE Journal of Civil Engineering*, Vol. 21, No. 3, pp. 792-806, 2017.
- [7] D. Chen, J. Yang, S. Kitipornchai, Nonlinear vibration and postbuckling of functionally graded graphene reinforced porous nanocomposite beams, *Composites Science and Technology*, Vol. 142, pp. 235-245, 2017.
- [8] A. M. Zenkour, A quasi-3D refined theory for functionally graded single-layered and sandwich plates with porosities, *Composite Structures*, Vol. 201, pp. 38-48, 2018.
- [9] E. Arshid, A. R. Khorshidvand, Free vibration analysis of saturated porous FG circular plates integrated with piezoelectric actuators via differential quadrature method, *Thin-Walled Structures*, Vol. 125, pp. 220-233, 2018.
- [10] B. Safaei, R. Moradi-Dastjerdi, K. Behdian, Z. Qin, F. Chu, Thermoelastic behavior of sandwich plates with porous polymeric core and CNT clusters/polymer nanocomposite layers, *Composite Structures*, Vol. 226, pp. 111209, 2019.
- [11] E. Arshid, S. Amir, A. Loghman, Static and dynamic analyses of FG-GNPs reinforced porous nanocomposite annular micro-plates based on MSGT, *International Journal of Mechanical Sciences*, Vol. 180, pp. 105656, 2020.
- [12] W. Gao, Z. Qin, F. Chu, Wave propagation in functionally graded porous plates reinforced with graphene platelets, *Aerospace Science and Technology*, Vol. 102, pp. 105860, 2020.
- [13] M. Askari, A. Saidi, A. Rezaei, An investigation over the effect of piezoelectricity and porosity distribution on natural frequencies of porous smart plates, *Journal of Sandwich Structures & Materials*, Vol. 22, No. 7, pp. 2091-2124, 2020.
- [14] M. Balak, S. J. Mehrabadi, H. M. Monfared, H. Feizabadi, Free vibration analysis of a composite elliptical plate made of a porous core and two piezoelectric layers, *Proceedings of the Institution of Mechanical Engineers, Part L: Journal of Materials: Design and Applications*, Vol. 235, No. 4, pp. 796-812, 2021.
- [15] M. Safari, M. Mohammadimehr, H. Ashrafi, Free vibration of electro-magneto-thermo sandwich Timoshenko beam made of porous core and GPLRC, *Advances in nano research*, Vol. 10, No. 2, pp. 115-128, 2021.
- [16] M. R. Ebrahimian, Z. Azimzadeh, A. Fatahi-Vajari, M. Shariati, Nonlinear coupled torsional-radial vibration of single-walled carbon nanotubes using numerical methods, *Journal of Computational Applied Mechanics*, Vol. 52, No. 4, pp. 642-663, 2021.
- [17] M. Shariati, M. Shishesaz, R. Mosalmani, S. A. Seyed Roknizadeh, M. Hosseini, Nonlocal effect on the axisymmetric nonlinear vibrational response of nano-disks using variational iteration method, *Journal of Computational Applied Mechanics*, Vol. 52, No. 3, pp. 507-534, 2021.
- [18] M. Shariati, M. Shishesaz, H. Sahbafar, M. Pourabdy, M. Hosseini, A review on stress-driven nonlocal elasticity theory, *Journal of Computational Applied Mechanics*, Vol. 52, No. 3, pp. 535-552, 2021.
- [19] S. R. Asemi, M. Mohammadi, A. Farajpour, A study on the nonlinear stability of orthotropic single-layered graphene sheet based on nonlocal elasticity theory, *Latin American Journal of Solids and Structures*, Vol. 11, pp. 1541-1546, 2014.
- [20] M. Baghani, M. Mohammadi, A. Farajpour, Dynamic and stability analysis of the rotating nanobeam in a nonuniform magnetic field considering the surface energy, *International Journal of Applied Mechanics*, Vol. 8, No. 04, pp. 1650048, 2016.
- [21] M. Danesh, A. Farajpour, M. Mohammadi, Axial vibration analysis of a tapered nanorod based on nonlocal elasticity theory and differential quadrature method, *Mechanics Research Communications*, Vol. 39, No. 1, pp. 23-27, 2012.
- [22] A. Farajpour, M. Danesh, M. Mohammadi, Buckling analysis of variable thickness nanoplates using nonlocal continuum mechanics, *Physica E: Low-dimensional Systems and Nanostructures*, Vol. 44, No. 3, pp. 719-727, 2011.

- [23] A. Farajpour, M. Mohammadi, A. Shahidi, M. Mahzoon, Axisymmetric buckling of the circular graphene sheets with the nonlocal continuum plate model, *Physica E: Low-dimensional Systems and Nanostructures*, Vol. 43, No. 10, pp. 1820-1825, 2011.
- [24] A. Farajpour, A. Shahidi, M. Mohammadi, M. Mahzoon, Buckling of orthotropic micro/nanoscale plates under linearly varying in-plane load via nonlocal continuum mechanics, *Composite Structures*, Vol. 94, No. 5, pp. 1605-1615, 2012.
- [25] M. Mohammadi, A. Farajpour, A. Moradi, M. Hosseini, Vibration analysis of the rotating multilayer piezoelectric Timoshenko nanobeam, *Engineering Analysis with Boundary Elements*, Vol. 145, pp. 117-131, 2022/12/01/, 2022.
- [26] H.-S. Shen, Nonlinear bending of functionally graded carbon nanotube-reinforced composite plates in thermal environments, *Composite Structures*, Vol. 91, No. 1, pp. 9-19, 2009.
- [27] L.-L. Ke, J. Yang, S. Kitipornchai, Nonlinear free vibration of functionally graded carbon nanotube-reinforced composite beams, *Composite Structures*, Vol. 92, No. 3, pp. 676-683, 2010.
- [28] H.-S. Shen, Postbuckling of nanotube-reinforced composite cylindrical shells in thermal environments, Part I: Axially-loaded shells, *Composite Structures*, Vol. 93, No. 8, pp. 2096-2108, 2011.
- [29] J. Jam, A. Pourasghar, S. Kamarian, Effect of the aspect ratio and waviness of carbon nanotubes on the vibrational behavior of functionally graded nanocomposite cylindrical panels, *Polymer Composites*, Vol. 33, No. 11, pp. 2036-2044, 2012.
- [30] A. Pourasghar, M. Yas, S. Kamarian, Local aggregation effect of CNT on the vibrational behavior of four-parameter continuous grading nanotube-reinforced cylindrical panels, *Polymer Composites*, Vol. 34, No. 5, pp. 707-721, 2013.
- [31] L. Zhang, B. Selim, Vibration analysis of CNT-reinforced thick laminated composite plates based on Reddy's higher-order shear deformation theory, *Composite Structures*, Vol. 160, pp. 689-705, 2017.
- [32] L. Zhang, Z. Lei, K. Liew, Vibration characteristic of moderately thick functionally graded carbon nanotube reinforced composite skew plates, *Composite Structures*, Vol. 122, pp. 172-183, 2015.
- [33] P. T. Thang, T.-T. Nguyen, J. Lee, A new approach for nonlinear buckling analysis of imperfect functionally graded carbon nanotube-reinforced composite plates, *Composites Part B: Engineering*, Vol. 127, pp. 166-174, 2017.
- [34] R. Moradi-Dastjerdi, F. Aghadavoudi, Static analysis of functionally graded nanocomposite sandwich plates reinforced by defected CNT, *Composite Structures*, Vol. 200, pp. 839-848, 2018.
- [35] H. Daghigh, V. Daghigh, A. Milani, D. Tannant, T. E. Lacy Jr, J. Reddy, Nonlocal bending and buckling of agglomerated CNT-reinforced composite nanoplates, *Composites Part B: Engineering*, Vol. 183, pp. 107716, 2020.
- [36] H. Asemi, S. Asemi, A. Farajpour, M. Mohammadi, Nanoscale mass detection based on vibrating piezoelectric ultrathin films under thermo-electro-mechanical loads, *Physica E: Low-dimensional Systems and Nanostructures*, Vol. 68, pp. 112-122, 2015.
- [37] S. Asemi, A. Farajpour, H. Asemi, M. Mohammadi, Influence of initial stress on the vibration of double-piezoelectric-nanoplate systems with various boundary conditions using DQM, *Physica E: Low-dimensional Systems and Nanostructures*, Vol. 63, pp. 169-179, 2014.
- [38] S. Asemi, A. Farajpour, M. Mohammadi, Nonlinear vibration analysis of piezoelectric nanoelectromechanical resonators based on nonlocal elasticity theory, *Composite Structures*, Vol. 116, pp. 703-712, 2014.
- [39] A. M. Zenkour, Hygrothermal analysis of heterogeneous piezoelectric elastic cylinders, *Mathematical Models in Engineering*, Vol. 2, No. 1, pp. 1-17, 2016.
- [40] M. Arefi, R. Karroubi, M. Irani-Rahaghi, Free vibration analysis of functionally graded laminated sandwich cylindrical shells integrated with piezoelectric layer, *Applied Mathematics and Mechanics*, Vol. 37, No. 7, pp. 821-834, 2016.
- [41] M. Ghasemi Shiri, A. Jaamialahmadi, Buckling Analysis of intelligent Nanoplate under Inplane Loading Based on Nonlocal Elasticity and Shear and normal Deformation Theories, *Modares Mechanical Engineering*, Vol. 17, No. 2, pp. 427-438, 2017.
- [42] M. Arefi, A. M. Zenkour, Vibration and bending analysis of a sandwich microbeam with two integrated piezo-magnetic face-sheets, *Composite Structures*, Vol. 159, pp. 479-490, 2017.
- [43] F. Ebrahimi, S. H. S. Hosseini, Investigation of flexoelectric effect on nonlinear forced vibration of piezoelectric/functionally graded porous nanocomposite resting on viscoelastic foundation, *The Journal of Strain Analysis for Engineering Design*, Vol. 55, No. 1-2, pp. 53-68, 2020.

- [44] A. G. Arani, A. Farazin, M. Mohammadimehr, S. Lenjannejadian, Energy harvesting of sandwich beam with laminated composite core and piezoelectric face sheets under external fluid flow, *Smart Structures and Systems*, Vol. 27, No. 4, pp. 641-650, 2021.
- [45] A. M. Zenkour, On vibration of functionally graded plates according to a refined trigonometric plate theory, *International Journal of Structural Stability and Dynamics*, Vol. 5, No. 02, pp. 279-297, 2005.
- [46] A. Zenkour, Benchmark trigonometric and 3-D elasticity solutions for an exponentially graded thick rectangular plate, *Archive of Applied Mechanics*, Vol. 77, No. 4, pp. 197-214, 2007.
- [47] M. Levy, Mémoire sur la théorie des plaques élastiques planes, *Journal de mathématiques pures et appliquées*, pp. 219-306, 1877.
- [48] M. Stein, Nonlinear theory for plates and shells including the effects of transverse shearing, *AIAA journal*, Vol. 24, No. 9, pp. 1537-1544, 1986.
- [49] A. Zenkour, M. Allam, A. Radwan, H. El-Mekawy, Thermo-mechanical bending response of exponentially graded thick plates resting on elastic foundations, *International Journal of Applied Mechanics*, Vol. 7, No. 04, pp. 1550062, 2015.
- [50] A. M. Zenkour, Bending analysis of functionally graded sandwich plates using a simple four-unknown shear and normal deformations theory, *Journal of Sandwich Structures & Materials*, Vol. 15, No. 6, pp. 629-656, 2013.
- [51] M. H. Sadd, 2009, *Elasticity: theory, applications, and numerics*, Academic Press,
- [52] D. Chen, S. Kitipornchai, J. Yang, Nonlinear free vibration of shear deformable sandwich beam with a functionally graded porous core, *Thin-Walled Structures*, Vol. 107, pp. 39-48, 2016.
- [53] M. Biot, Theory of buckling of a porous slab and its thermoelastic analogy, 1964.
- [54] J. D. Eshelby, The determination of the elastic field of an ellipsoidal inclusion, and related problems, *Proceedings of the royal society of London. Series A. Mathematical and physical sciences*, Vol. 241, No. 1226, pp. 376-396, 1957.
- [55] T. Mori, K. Tanaka, Average stress in matrix and average elastic energy of materials with misfitting inclusions, *Acta metallurgica*, Vol. 21, No. 5, pp. 571-574, 1973.
- [56] R. Hill, A self-consistent mechanics of composite materials, *Journal of the Mechanics and Physics of Solids*, Vol. 13, No. 4, pp. 213-222, 1965.
- [57] A. G. Arani, H. K. Arani, Z. K. Maraghi, Vibration analysis of sandwich composite micro-plate under electro-magneto-mechanical loadings, *Applied Mathematical Modelling*, Vol. 40, No. 23-24, pp. 10596-10615, 2016.
- [58] A. Ghorbanpour Arani, M. Zamani, Investigation of electric field effect on size-dependent bending analysis of functionally graded porous shear and normal deformable sandwich nanoplate on silica Aerogel foundation, *Journal of Sandwich Structures & Materials*, Vol. 21, No. 8, pp. 2700-2734, 2019.
- [59] J. N. Reddy, 2017, *Energy principles and variational methods in applied mechanics*, John Wiley & Sons,
- [60] M. Arefi, A. H. Soltan Arani, Higher order shear deformation bending results of a magneto-electrothermoelastic functionally graded nanobeam in thermal, mechanical, electrical, and magnetic environments, *Mechanics Based Design of Structures and Machines*, Vol. 46, No. 6, pp. 669-692, 2018.
- [61] J. Reddy, Nonlocal theories for bending, buckling and vibration of beams, *International journal of engineering science*, Vol. 45, No. 2-8, pp. 288-307, 2007.
- [62] S. Srinivas, C. J. Rao, A. Rao, An exact analysis for vibration of simply-supported homogeneous and laminated thick rectangular plates, *Journal of sound and vibration*, Vol. 12, No. 2, pp. 187-199, 1970.
- [63] J. Reddy, N. Phan, Stability and vibration of isotropic, orthotropic and laminated plates according to a higher-order shear deformation theory, *Journal of sound and vibration*, Vol. 98, No. 2, pp. 157-170, 1985.
- [64] H. Hebali, A. Tounsi, M. S. A. Houari, A. Bessaim, E. A. A. Bedia, New quasi-3D hyperbolic shear deformation theory for the static and free vibration analysis of functionally graded plates, *Journal of Engineering Mechanics*, Vol. 140, No. 2, pp. 374-383, 2014.
- [65] Z.-X. Wang, H.-S. Shen, Nonlinear vibration and bending of sandwich plates with nanotube-reinforced composite face sheets, *Composites Part B: Engineering*, Vol. 43, No. 2, pp. 411-421, 2012.
- [66] A. W. Leissa, The free vibration of rectangular plates, *Journal of sound and vibration*, Vol. 31, No. 3, pp. 257-293, 1973.
- [67] N. Bardell, The application of symbolic computing to the hierarchical finite element method, *International Journal for Numerical Methods in Engineering*, Vol. 28, No. 5, pp. 1181-1204, 1989.
- [68] X. Wang, Y. L. Wang, R. B. Chen, Static and free vibrational analysis of rectangular plates by the differential quadrature element method, *Communications in Numerical Methods in Engineering*, Vol. 14, No. 12, pp. 1133-1141, 1998.

- [69] H. Akhavan, S. H. Hashemi, H. R. D. Taher, A. Alibeigloo, S. Vahabi, Exact solutions for rectangular Mindlin plates under in-plane loads resting on Pasternak elastic foundation. Part II: Frequency analysis, *Computational Materials Science*, Vol. 44, No. 3, pp. 951-961, 2009.
- [70] H. A. Atmane, A. Tounsi, I. Mechab, Free vibration analysis of functionally graded plates resting on Winkler–Pasternak elastic foundations using a new shear deformation theory, *International Journal of Mechanics and Materials in Design*, Vol. 6, No. 2, pp. 113-121, 2010.
- [71] R. Moradi-Dastjerdi, G. Payganeh, H. Malek-Mohammadi, Free vibration analyses of functionally graded CNT reinforced nanocomposite sandwich plates resting on elastic foundation, *Journal of Solid Mechanics*, Vol. 7, No. 2, pp. 158-172, 2015.
- [72] Q. Li, V. Iu, K. Kou, Three-dimensional vibration analysis of functionally graded material sandwich plates, *Journal of Sound and Vibration*, Vol. 311, No. 1-2, pp. 498-515, 2008.
- [73] M. Arefi, M. Zamani, M. Kiani, Size-dependent free vibration analysis of three-layered exponentially graded nanoplate with piezomagnetic face-sheets resting on Pasternak’s foundation, *Journal of Intelligent Material Systems and Structures*, Vol. 29, No. 5, pp. 774-786, 2018.
- [74] A. G. Arani, S. Maghamikia, M. Mohammadimehr, A. Arefmanesh, Buckling analysis of laminated composite rectangular plates reinforced by SWCNTs using analytical and finite element methods, *Journal of mechanical science and technology*, Vol. 25, No. 3, pp. 809-820, 2011.
- [75] S. Amir, E. Arshid, S. A. Rasti-Alhosseini, A. Loghman, Quasi-3D tangential shear deformation theory for size-dependent free vibration analysis of three-layered FG porous micro rectangular plate integrated by nanocomposite faces in hygrothermal environment, *Journal of Thermal Stresses*, Vol. 43, No. 2, pp. 133-156, 2020.
- [76] A. Ghorbanpour Arani, H. BabaAkbar Zarei, E. Haghparast, Vibration response of viscoelastic sandwich plate with magnetorheological fluid core and functionally graded-piezoelectric nanocomposite face sheets, *Journal of Vibration and Control*, Vol. 24, No. 21, pp. 5169-5185, 2018.